buildings

MDPI

Article

Longitudinal Dynamic Response of End-Bearing Piles in Radially Heterogeneous Unsaturated Soil

Cun Zhang [1,2], Renhao Lin [1,2], Peiqing Wang [1,2], Li Wan [3] and Zhenya Li [4,*]

[1] College of Water Conservancy and Civil Engineering, Xizang Agricultural and Animal Husbandry University, Linzhi 860000, China; zhangcun@xza.edu.cn (C.Z.); 202400501284@stu.xza.edu.cn (R.L.); 19951015@xza.edu.cn (P.W.)
[2] Research Center of Civil, Hydraulic and Power Engineering of Xizang, Xizang Agricultural and Animal Husbandry University, Linzhi 860000, China
[3] Xizang Autonomous Region Energy Research and Demonstration Center, Lasa 850000, China; xizangnengyuan@163.com
[4] Key Laboratory of Ministry of Education for Geomechanics and Embankment Engineering, Hohai University, Nanjing, 210098, China
* Correspondence: jllizhenya@163.com

Abstract

This study investigates the longitudinal dynamic response of end-bearing piles embedded in radially heterogeneous unsaturated soil induced by construction disturbance. The unsaturated soil is described using the theory of motion for three-phase poroelastic media, while the radial inhomogeneity of the surrounding soil is represented by the complex shear stiffness transfer model. The soil is discretized into concentric vertical annular zones, each of which is assumed to be homogeneous, while soil properties may differ between adjacent zones. The governing equations for each soil zone are then solved and coupled with the pile governing equation to derive an analytical solution for the pile-head complex impedance. After validating the proposed solution, a parametric analysis is conducted to examine how pile–soil parameters affect the longitudinal dynamic response of end-bearing piles in radially heterogeneous unsaturated soil.

Keywords: longitudinal vibration; unsaturated soil; construction disturbance; radial heterogeneity; complex impedance

Check for updates

Academic Editor: Eugeniusz Koda

Received: 2 October 2026
Revised: 13 November 2026
Accepted: 16 November 2026
Published: 18 November 2026

Copyright: © 2026 by the authors. Licensee MDPI, Basel, Switzerland. This article is an open access article distributed under the terms and conditions of the Creative Commons Attribution (CC BY) license.

1. Introduction

Pile foundations are widely used in engineering practice because they provide high load-bearing capacity [1] and favourable seismic performance [2]. Throughout their operational period, pile foundations experience a combination of static loads and, in many practical scenarios, axial dynamic loading [3,4]. Because axial pile vibration theory provides a fundamental basis for both the dynamic design of pile foundations and the evaluation of pile integrity [5,6], it has attracted sustained attention over the past several decades. A range of analytical approaches [7,8] and numerical methods [9–11] have consequently been developed. Existing models of pile–soil dynamic interaction can be broadly classified into three categories: Winkler-type models [12–14], plane-strain models [15–17], and three-dimensional axisymmetric models [18–20]. The continuing refinement of these models has substantially advanced the theoretical understanding of pile vibration.

Notably, previous studies have generally treated the soil surrounding the piles as either a single-phase medium [21–23] or a two-phase saturated medium [24–26], whereas comparatively little attention has been paid to unsaturated soils. In natural settings, however,

most soils are unsaturated and therefore constitute three-phase porous media composed of a solid skeleton, pore water and pore air. Compared with single-phase and saturated soils, unsaturated soils exhibit more complex and variable interactions among the three phases, leading to markedly different dynamic responses. Consequently, vibration theories developed for piles in single-phase or saturated soils cannot be directly extended to piles interacting with unsaturated ground, because both air bubbles [27] and matric suction [28] can effect pile–soil interaction. To address this problem, a theory of motion for three-phase poroelastic media was developed by extending Biot's theory of dynamic consolidation [29] to describe unsaturated soils. Within this theoretical framework, Wang et al. [30] investigated the vertical vibration response of an end-bearing pile subjected to vertical harmonic loading. Building on this work, Guo et al. [31] further incorporated the lateral inertia of the pile. Subsequently, Shan et al. [32] examined the vertical vibration of friction piles in homogeneous unsaturated soil using the fictitious unsaturated soil pile (FUSP) model, while Ma et al. [33] analyzed the vertical vibration of end-bearing piles in homogeneous unsaturated soil. In addition, several studies have addressed the horizontal vibration [34–38] and torsional vibration [39–42] of piles embedded in unsaturated soil.

During pile installation, disturbance of the surrounding soil is difficult to avoid. Such disturbance may densify or loosen the soil, thereby inducing radial heterogeneity in its properties [43]; this phenomenon is commonly referred to as construction disturbance. To represent the radial heterogeneity caused by such disturbance, several models have been proposed [44–47], among which the complex shear stiffness transfer model proposed by [48] is the most widely used. The central idea of this model is to divide the soil into a series of concentric vertical annular zones. Soil properties vary from one zone to another in the radial direction, whereas the soil within each zone is assumed to be homogeneous. Each zone is governed by its own field equation, and the coupled system is solved recursively through the transfer of shear stiffness between adjacent zones, enabling the dynamic pile–soil interaction to be determined. Using this approach, researchers have combined the complex shear stiffness transfer model with Biot's theory and its extensions to investigate the effects of construction disturbance in saturated and unsaturated soils [49–52]. Collectively, these studies show that construction disturbance has a pronounced effect on the vertical vibration characteristics of piles.

Existing analyses of longitudinal pile vibration in unsaturated soils generally assume homogeneous conditions, while studies incorporating radial heterogeneity mainly consider single-phase or saturated soils, leaving the coupled effects of the solid skeleton, pore water, and pore air insufficiently addressed. To bridge this gap, this study integrates the governing equations of three-phase unsaturated poroelastic media with a complex shear-stiffness transfer scheme to develop an analytical framework for the longitudinal vibration of an end-bearing pile in construction-disturbed, radially heterogeneous unsaturated soil. The framework extends existing formulations and enables systematic investigation of how soil saturation, radial disturbance extent and intensity, and pile properties jointly influence the frequency-dependent complex impedance at the pile head.

Contribution and Scope

The contribution of this study is to extend longitudinal pile vibration analysis in homogeneous unsaturated soil to radially heterogeneous conditions, considering both radial and vertical skeleton displacements and solid–water–air coupling. Unlike previous disturbance-aware horizontal and torsional vibration studies, the formulation addresses axial pile–soil interaction and the resulting pile-head impedance. The analysis concerns small-amplitude vibration of a single pile with a rigidly restrained toe, with soil properties varying radially but remaining uniform with depth.

2. Mathematical Model and Governing Equations

2.1. Mathematical Model

The mathematical framework established for investigating pile–soil interaction in radially heterogeneous unsaturated soils is illustrated in Figure 1 The pile is characterized by a length H and a radius r_p, and a vertical harmonic excitation $P_0e^{i\omega t}$ is imposed at the pile head. Because construction disturbance inevitably gives rise to radial heterogeneity in the soil surrounding the pile. Following the methodology proposed by Li et al. [53], the soil domain is discretized into m concentric vertical annular layers along the radial direction, which are sequentially numbered from 1 to m. The inner boundary radius of the jth annular layer is represented by r_j.

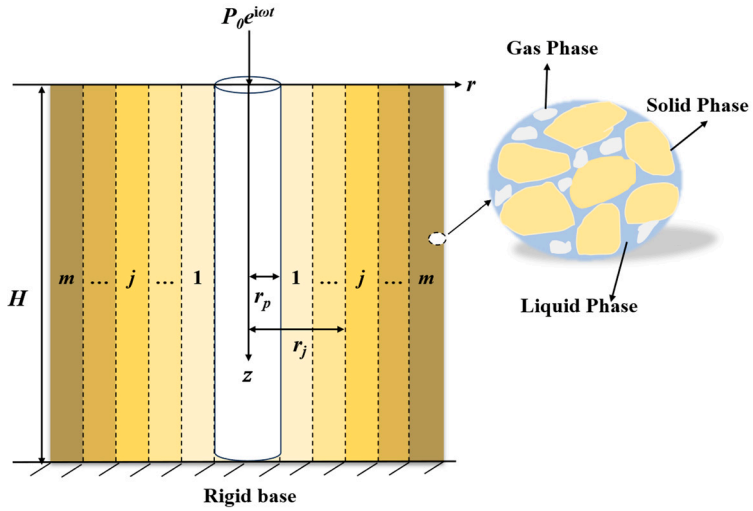


Figure 1. Pile–soil interaction model.

To enable the derivation and solution of the governing equations for the pile–soil interaction system, the following assumptions are adopted:

(1) Each vertical annular soil zone is assumed to be homogeneous, while its mechanical and hydraulic properties may differ from those of adjacent zones.

(2) The pile is idealized as a vertical cylindrical viscoelastic member, and its dynamic response is described using a one-dimensional model.

(3) Both vertical and radial components of soil displacement are incorporated into the analysis of unsaturated soil behavior.

(4) A fully bonded condition is assumed at the pile–soil interface and between neighboring annular soil layers; this idealization excludes slip and separation, ensuring the continuity of displacement and stress transmission across these interfaces.

(5) The ground surface is assumed to be a traction-free boundary that allows the free exchange of both pore water and pore air. At the underlying rigid base, soil deformation is completely constrained.

2.2. Governing Equations

Based on Xu and Wei [54] the dynamic governing equations for unsaturated soil established from the three-dimensional theory of motion for poroelastic media are expressed as follows:

$$G_s\nabla^2\mathbf{u} + (\lambda_c + G_s)\nabla(\nabla\cdot\mathbf{u}) + M\nabla(\nabla\cdot\mathbf{v}) + N\nabla(\nabla\cdot\mathbf{w}) = \rho\ddot{\mathbf{u}} + \rho_f\ddot{\mathbf{v}} + \rho_g\ddot{\mathbf{w}} \quad (1)$$

$$D_1\nabla(\nabla\cdot\mathbf{u}) + D_2\nabla(\nabla\cdot\mathbf{v}) + D_3\nabla(\nabla\cdot\mathbf{w}) = \rho_f\ddot{\mathbf{u}} + \vartheta_f\ddot{\mathbf{v}} + b_f\dot{\mathbf{v}} \quad (2)$$

$$D_4\nabla(\nabla\cdot\mathbf{u})+D_5\nabla(\nabla\cdot\mathbf{v})+D_6\nabla(\nabla\cdot\mathbf{w})=\rho_g\ddot{\mathbf{u}}+\vartheta_g\ddot{\mathbf{w}}+b_g\dot{\mathbf{w}} \tag{3}$$

The seepage-continuity equations can be written as:

$$p_f=D_1\nabla\cdot\mathbf{u}+D_2\nabla\cdot\mathbf{v}+D_3\nabla\cdot\mathbf{w} \tag{4}$$

$$p_g=D_4\nabla\cdot\mathbf{u}+D_5\nabla\cdot\mathbf{v}+D_6\nabla\cdot\mathbf{w} \tag{5}$$

where $\lambda_c=\lambda+a\gamma D_1+a(1-\gamma)D_4$; $M=a\gamma D_2+a(1-\gamma)D_5$; $N=a\gamma D_3+a(1-\gamma)D_6$; $\vartheta_f=\frac{\rho_f}{nS_r}$; $\vartheta_g=\frac{\rho_g}{n(1-S_r)}$; $b_f=\frac{\eta_f}{k_{rf}K_d}$; $b_g=\frac{\eta_g}{k_{rg}K_d}$; $k_{rf}=\sqrt{S_e}\left\{1-\left[1-(S_e)^{\frac{1}{m_1}}\right]^{m_1}\right\}^2$; $k_{rg}=\sqrt{1-S_e}\left[1-(S_e)^{\frac{1}{m_1}}\right]^{2m_1}$; $S_e=\frac{S_r-S_{w0}}{1-S_{w0}}$; $\rho=(1-n)\rho_s+nS_r\rho_f+n(1-S_r)\rho_g D_1=\frac{aA_{22}}{A_{11}A_{22}-A_{12}A_{21}}$; $D_2=\frac{1}{nS_r}\frac{A_{22}A_{13}-A_{12}A_{23}}{A_{11}A_{22}-A_{12}A_{21}}$; $D_3=\frac{1}{n(1-S_r)}\frac{A_{22}A_{14}-A_{12}A_{24}}{A_{11}A_{22}-A_{12}A_{21}}$; $D_4=-\frac{aA_{21}}{A_{11}A_{22}-A_{12}A_{21}}$; $D_5=\frac{1}{nS_r}\frac{A_{11}A_{23}-A_{21}A_{13}}{A_{11}A_{22}-A_{12}A_{21}}$; $D_6=\frac{1}{n(1-S_r)}\frac{A_{11}A_{24}-A_{21}A_{14}}{A_{11}A_{22}-A_{12}A_{21}}$; $A_{11}=\frac{a\gamma-nS_r}{K_s}+\frac{nS_r}{K_f}$; $A_{12}=\frac{a(1-\gamma)-n(1-S_r)}{K_s}+\frac{n(1-S_r)}{K_g}$; $A_{13}=nS_r$; $A_{14}=n(1-S_r)$; $A_{21}=A_s-\frac{S_r(1-S_r)}{K_f}$; $A_{22}=\frac{S_r(1-S_r)}{K_g}-A_s$; $A_{23}=-A_{24}=-S_r(1-S_r)$; $A_s=-\chi m_1 d(1-S_{w0})(S_e)^{\frac{m_1+1}{m_1}}\left[(S_e)^{-\frac{1}{m_1}}-1\right]^{\frac{d-1}{d}}$; $\gamma=S_r$; $a=1-\frac{K_b}{K_s}$; $K_b=\lambda+\frac{2}{3}G$.

Where **u** denotes the displacement vector of the soil skeleton, whereas **v** and **w** represent the relative displacement vectors of the pore water and pore gas phases with respect to the solid phase, respectively. A dot placed above a variable indicates its time derivative. The quantities λ_c and G_s are the Lamé parameters of the soil skeleton. Throughout the following equations, the subscripts s, f and g refer to the solid, fluid, and gas constituents of the unsaturated soil, respectively. The symbols ρ, ρ_s, ρ_f and ρ_g represent the densities of the soil mixture, soil grains, pore water, and pore gas phases, respectively. The variables S_r, n and K_d denote the degree of saturation, porosity, and intrinsic permeability of the unsaturated soil, respectively. The parameters η_f and η_g describe the dynamic viscosities of pore water and pore gas, while k_{rf} and k_{rg} indicate their corresponding relative permeability coefficients. In addition, K_s, K_f, K_g and K_b represent the bulk moduli of the soil particles, pore water, pore gas, and soil skeleton, respectively. The coefficients A_s, χ, m_1 and d are empirical parameters introduced for model fitting.

Expanding vector Equations (1)–(3) in a cylindrical coordinate system and considering the axisymmetric nature of the pile–soil interaction model yields the following governing equations:

$$G_{sj}\left(\nabla^2-\frac{1}{r^2}\right)u_{rj}+\left(\lambda_{cj}+G_{sj}\right)\frac{\partial e}{\partial r}+M_j\frac{\partial\zeta}{\partial r}+N_j\frac{\partial\xi}{\partial r}=\rho_j\ddot{u}_{rj}+\rho_{fj}\ddot{v}_{rj}+\rho_{gj}\ddot{w}_{rj} \tag{6}$$

$$G_{sj}\nabla^2u_{zj}+\left(\lambda_{cj}+G_{sj}\right)\frac{\partial e}{\partial z}+M_j\frac{\partial\zeta}{\partial z}+N_j\frac{\partial\xi}{\partial z}=\rho_j\ddot{u}_{zj}+\rho_{fj}\ddot{v}_{zj}+\rho_{gj}\ddot{w}_{zj} \tag{7}$$

$$D_{1j}\frac{\partial e}{\partial r}+D_{2j}\frac{\partial\zeta}{\partial r}+D_{3j}\frac{\partial\xi}{\partial r}=\rho_{fj}\ddot{u}_{rj}+\vartheta_{fj}\ddot{v}_{rj}+b_{fj}\dot{v}_{rj} \tag{8}$$

$$D_{1j}\frac{\partial e}{\partial z}+D_{2j}\frac{\partial\zeta}{\partial z}+D_{3j}\frac{\partial\xi}{\partial z}=\rho_{fj}\ddot{u}_{zj}+\vartheta_{fj}\ddot{v}_{zj}+b_{fj}\dot{v}_{zj} \tag{9}$$

$$D_{4j}\frac{\partial e}{\partial r}+D_{5j}\frac{\partial\zeta}{\partial r}+D_{6j}\frac{\partial\xi}{\partial r}=\rho_{gj}\ddot{u}_{rj}+\vartheta_{gj}\ddot{v}_{rj}+b_{gj}\dot{v}_{rj} \tag{10}$$

$$D_{4j}\frac{\partial e}{\partial z}+D_{5j}\frac{\partial\zeta}{\partial z}+D_{6j}\frac{\partial\xi}{\partial z}=\rho_{gj}\ddot{u}_{zj}+\vartheta_{gj}\ddot{v}_{zj}+b_{gj}\dot{v}_{zj} \tag{11}$$

Stress–strain constitutive equations are given as follows:

$$\sigma_{zj}=\lambda_{cj}e+2G_{sj}\frac{\partial u_{zj}}{\partial z}-ap_j \tag{12}$$

$$\tau_{zrj}=G_{sj}\left(\frac{\partial u_{rj}}{\partial z}+\frac{\partial u_{zj}}{\partial r}\right) \tag{13}$$

$$p_{fj} = -D_{1j}e - D_{2j}\zeta - D_{3j}\xi \tag{14}$$

$$p_{gj} = -D_{4j}e - D_{5j}\zeta - D_{6j}\xi \tag{15}$$

where $\nabla^2 = \frac{\partial^2}{\partial r^2} + \frac{1}{r}\frac{\partial}{\partial r} + \frac{\partial^2}{\partial z^2}$ denotes the Laplace operator, and e, ζ and ξ denote the volumetric deformation of the soil skeleton and the relative volumetric strains of the pore water and pore gas phases with respect to the soil skeleton, respectively, expressed as $e = \frac{\partial u_{rj}}{\partial r} + \frac{u_{rj}}{r} + \frac{\partial u_{zj}}{\partial z}$, $\zeta = \frac{\partial v_{rj}}{\partial r} + \frac{v_{rj}}{r} + \frac{\partial v_{zj}}{\partial z}$, $\xi = \frac{\partial w_{rj}}{\partial r} + \frac{w_{rj}}{r} + \frac{\partial w_{zj}}{\partial z}$.

Under vertical harmonic loading, the vertical displacement of the viscoelastic pile can be expressed as $u_p(z)e^{i\omega t}$; therefore, the governing equation for vertical vibration of the pile can be written as follows:

$$E_p A_p \frac{\partial^2}{\partial z^2}[u_p(z)e^{i\omega t}] + A_p \delta_p \frac{\partial^3}{\partial z^2 \partial t}[u_p(z)e^{i\omega t}] - \rho_p A_p \frac{\partial^2}{\partial t^2}[u_p(z)e^{i\omega t}] - 2\pi r_1 f(r_1, z)e^{i\omega t} = 0 \tag{16}$$

where $u_p(z)$, E_p, A_p, ρ_p, and δ_p are the corresponding parameters describing the amplitude of vertical pile displacement, Young's modulus, cross-sectional area, density, and damping coefficient of the pile material, respectively. In addition, $f(r_1,z)$ represents the amplitude of the soil-induced shear stress acting along the pile shaft.

2.3. Boundary Conditions

The boundary conditions imposed at the foundation base are given as follows:

$$u_{rj}\big|_{z=H} = v_{rj}\big|_{z=H} = w_{rj}\big|_{z=H} = u_{zj}\big|_{z=H} = v_{zj}\big|_{z=H} = w_{zj}\big|_{z=H} = 0 \tag{17}$$

The radial soil displacement approaches zero at an infinite radial distance:

$$u_{rj}\big|_{r=\infty} = v_{rj}\big|_{r=\infty} = w_{rj}\big|_{r=\infty} = u_{zj}\big|_{r=\infty} = v_{zj}\big|_{r=\infty} = w_{zj}\big|_{r=\infty} = 0 \tag{18}$$

The ground surface is permeable to water and air, and the normal stress is zero.

$$\begin{cases} p_{fj}(r,0) = p_{gj}(r,0) = 0 \\ \sigma_{zj}(r,0) = 0 \end{cases} \tag{19}$$

According to the continuity conditions for stress and displacement between adjacent soil annular zones, we have:

$$\begin{cases} u_{rj}(r_{j+1},z) = u_{r(j+1)}(r_{j+1},z) \\ v_{rj}(r_{j+1},z) = v_{r(j+1)}(r_{j+1},z) \\ w_{rj}(r_{j+1},z) = w_{r(j+1)}(r_{j+1},z) \end{cases} \tag{20}$$

$$\begin{cases} u_{zj}(r_{j+1},z) = u_{z(j+1)}(r_{j+1},z) \\ v_{zj}(r_{j+1},z) = v_{z(j+1)}(r_{j+1},z) \\ w_{zj}(r_{j+1},z) = w_{z(j+1)}(r_{j+1},z) \end{cases} \tag{21}$$

$$\begin{cases} \tau_{zrj}(r_{j+1},z) = \tau_{zr(j+1)}(r_{j+1},z) \\ \sigma_{zj}(r_{j+1},z) = \sigma_{z(j+1)}(r_{j+1},z) \end{cases} \tag{22}$$

The boundary conditions at the pile head and pile tip are respectively expressed as follows:

$$\left(E_p A_p + A_p \delta_p i\omega\right)\frac{\mathrm{d}u_p(z)}{\mathrm{d}z}\bigg|_{z=0} = -P_0 \tag{23}$$

$$u_p(z)\big|_{z=H} = 0 \tag{24}$$

where P_0 is the amplitude of the excitation force applied at the pile head.

Pile–soil interface continuity conditions:

$$u_{r1}(r_1,z) = v_{r1}(r_1,z) = w_{r1}(r_1,z) = 0 \tag{25}$$

$$u_{z1}(r,z)\big|_{r=r_1} = u_p(z) \tag{26}$$

$$f(r,z)\big|_{r=r_1} = -\tau_{rz1}(r,z)\big|_{r=r_1} \tag{27}$$

3. Solution of the Equations

3.1. Solution of the Soil Governing Equations

For steady-state harmonic vibration, all variables vary harmonically with time. To facilitate the decoupled solution of the governing equations, a set of potential functions is introduced. Based on these potentials, the displacement vectors of the solid skeleton, pore water, and pore gas phases are formulated as follows:

$$u_{rj} = \frac{\partial \phi_{sj}}{\partial r} + \frac{\partial^2 \psi_{sj}}{\partial z \partial r}, u_{zj} = \frac{\partial \phi_{sj}}{\partial z} - \frac{1}{r}\frac{\partial}{\partial r}\left(r\frac{\partial \psi_{sj}}{\partial r}\right) \tag{28}$$

$$v_{rj} = \frac{\partial \phi_{gj}}{\partial r} + \frac{\partial^2 \psi_{fj}}{\partial z \partial r}, v_{zj} = \frac{\partial \phi_{fj}}{\partial z} - \frac{1}{r}\frac{\partial}{\partial r}\left(r\frac{\partial \psi_{fj}}{\partial r}\right) \tag{29}$$

$$w_{rj} = \frac{\partial \phi_{gj}}{\partial r} + \frac{\partial^2 \psi_{gj}}{\partial z \partial r}, w_{zj} = \frac{\partial \phi_{gj}}{\partial z} - \frac{1}{r}\frac{\partial}{\partial r}\left(r\frac{\partial \psi_{gj}}{\partial r}\right) \tag{30}$$

where ϕ_{sj}, ψ_{sj}, ϕ_{fj}, ψ_{fj}, ϕ_{gj}, ψ_{gj} are the displacement scalar potentials of the solid, water and air phases, respectively.

The volumetric strains can be expressed as:

$$e = \nabla^2 \phi_{sj}, \zeta = \nabla^2 \phi_{fj}, \xi = \nabla^2 \phi_{gj} \tag{31}$$

Substituting Equations (28)–(30) into Equations (1)–(3) yields two independent matrix equations. For the scalar potentials:

$$\begin{bmatrix} b_{1j}\nabla^2 - \delta^2 & \overline{M}_j\nabla^2 - \overline{\rho}_{fj}\delta^2 & \overline{N}_j\nabla^2 - \overline{\rho}_{gj}\delta^2 \\ \overline{D}_{1j}\nabla^2 - \overline{\rho}_{fj}\delta^2 & \overline{D}_{2j}\nabla^2 - b_{2j} & \overline{D}_{3j}\nabla^2 \\ \overline{D}_{4j}\nabla^2 - \overline{\rho}_{gj}\delta^2 & \overline{D}_{5j}\nabla^2 & \overline{D}_{6j}\nabla^2 - b_{3j} \end{bmatrix} \begin{bmatrix} \overline{\phi}_{sj} \\ \overline{\phi}_{fj} \\ \overline{\phi}_{gj} \end{bmatrix} = \begin{bmatrix} 0 \\ 0 \\ 0 \end{bmatrix} \tag{32}$$

$$\begin{bmatrix} \nabla^2 - \delta^2 & -\overline{\rho}_{fj}\delta^2 & -\overline{\rho}_{gj}\delta^2 \\ \overline{\rho}_{fj}\delta^2 & b_{2j} & 0 \\ \overline{\rho}_{gj}\delta^2 & 0 & b_{3j} \end{bmatrix} \begin{bmatrix} \overline{\psi}_{sj} \\ \overline{\psi}_{fj} \\ \overline{\psi}_{gj} \end{bmatrix} = \begin{bmatrix} 0 \\ 0 \\ 0 \end{bmatrix} \tag{33}$$

where $\overline{\phi}_{sj}$, $\overline{\psi}_{sj}$, $\overline{\phi}_{fj}$, $\overline{\psi}_{fj}$, $\overline{\phi}_{gj}$, $\overline{\psi}_{gj}$ are the Laplace transforms of the displacement scalar potentials ϕ_{sj}, ψ_{sj}, ϕ_{fj}, ψ_{fj}, ϕ_{gj}, ψ_{gj} respectively; $b_{1j} = \overline{\lambda}_{cj}+2$, $b_{2j} = \overline{\vartheta}_{fj}\delta^2+\overline{b}_{fj}\delta$, $b_{3j} = \overline{\vartheta}_{gj}\delta^2+\overline{b}_{gj}\delta$. The overbar in the above equations denotes the dimensionless form of each variable, and $\overline{\lambda}_{cj} = \lambda_{cj}/G_{sj}$, $\overline{M}_j = M_j/G_{sj}$, $\overline{N}_j = N_j/G_{sj}$, $\overline{D}_{nj} = D_{nj}/G_{sj} (n = 1, 2, \cdots, 6)$ $\overline{\rho}_f = \rho_f/\rho$, $\overline{\rho}_{gj} = \rho_{gj}/\rho_j$, $\overline{\vartheta}_{fj} = \vartheta_{fj}/\rho_j$, $\overline{\vartheta}_{gj} = \vartheta_{gj}/\rho_j$, $\overline{b}_{fj} = b_{fj}r_1/\sqrt{\rho_j G_{sj}}$, $\overline{b}_{gj} = b_{gj}r_1/\sqrt{\rho_j G_{sj}}$, $\delta = r_1 s\sqrt{\rho_j/G_{sj}}$.

For Equations (32) and (33) to admit nontrivial solutions, the determinant of the corresponding coefficient matrix must be zero. Therefore, we obtain:

$$\begin{cases} (h_{1j}(\nabla^2)^3 + h_{2j}(\nabla^2)^2 + h_{3j}\nabla^2 + h_{4j})\overline{\phi}_{sj} = 0 \\ (h_{1j}(\nabla^2)^3 + h_{2j}(\nabla^2)^2 + h_{3j}\nabla^2 + h_{4j})\overline{\phi}_{fj} = 0 \\ (h_{1j}(\nabla^2)^3 + h_{2j}(\nabla^2)^2 + h_{3j}\nabla^2 + h_{4j})\overline{\phi}_{gj} = 0 \end{cases} \tag{34}$$

$$\begin{cases} (\nabla^2 - \beta_{4j}^2)\overline{\psi}_{sj} = 0 \\ (\nabla^2 - \beta_{4j}^2)\overline{\psi}_{fj} = 0 \\ (\nabla^2 - \beta_{4j}^2)\overline{\psi}_{gj} = 0 \end{cases} \tag{35}$$

The coefficients in Equations (34) and (35) are as follows:

$$
\begin{aligned}
&h_{1j} = b_{1j}(\overline{D}_{2j}\overline{D}_{6j} - \overline{D}_{3j}\overline{D}_{5j}) + \overline{M}_j(\overline{D}_{3j}\overline{D}_{4j} - \overline{D}_{1j}\overline{D}_{6j}) + \overline{N}_j(\overline{D}_{1j}\overline{D}_{5j} - \overline{D}_{2j}\overline{D}_{4j});\\
&h_{2j} = -\overline{\rho}_{fj}\delta^2(\overline{D}_{3j}\overline{D}_{4j} - \overline{D}_{1j}\overline{D}_{6j} + \overline{D}_{5j}\overline{N}_j - \overline{D}_{6j}\overline{M}_j) + b_{2j}(\overline{D}_{4j}\overline{N}_j - \overline{D}_{6j}b_{1j}) + b_{3j}(\overline{D}_{1j}\overline{M}_j - \overline{D}_{2j}b_{1j})\\
&\quad -\overline{\rho}_{gj}\delta^2(\overline{D}_{1j}\overline{D}_{5j} - \overline{D}_{2j}\overline{D}_{4j} + \overline{D}_{3j}\overline{M}_j - \overline{D}_{2j}\overline{N}_j) - \delta^2(\overline{D}_{2j}\overline{D}_{6j} - \overline{D}_{3j}\overline{D}_{5j});\\
&h_{3j} = \overline{\rho}_{fj}\overline{\rho}_{gj}\delta^4(\overline{D}_{3j} + \overline{D}_{5j}) - \overline{\rho}_{fj}^2\delta^4\overline{D}_{6j} - \overline{\rho}_{gj}^2\delta^4\overline{D}_{2j} - \overline{\rho}_{fj}\delta^2 b_{3j}(\overline{D}_{1j} + \overline{M}_j)\\
&\quad -\overline{\rho}_{gj}\delta^2 b_{2j}(\overline{D}_{4j} + \overline{N}_j) + \delta^2(\overline{D}_{2j}b_{3j} + \overline{D}_{6j}b_{2j}) + b_{1j}b_{2j}b_{3j};\\
&h_{4j} = \overline{\rho}_{fj}^2\delta^4 b_{3j} + \overline{\rho}_{gj}^2\delta^4 b_{2j} - \delta^2 b_{2j}b_{3j};\\
&\beta_{4j}^2 = \frac{-\overline{\rho}_{fj}^2\delta^4 b_{3j} - \overline{\rho}_{gj}^2\delta^4 b_{2j} + \delta^2 b_{2j}b_{3j}}{b_{2j}b_{3j}}.
\end{aligned}
$$

Equation (34) can be factorized as:

$$
\begin{cases}
\left(\nabla^2 - \beta_{1j}^2\right)\left(\nabla^2 - \beta_{2j}^2\right)\left(\nabla^2 - \beta_{3j}^2\right)\overline{\phi}_{sj} = 0\\
\left(\nabla^2 - \beta_{1j}^2\right)\left(\nabla^2 - \beta_{2j}^2\right)\left(\nabla^2 - \beta_{3j}^2\right)\overline{\phi}_{fj} = 0\\
\left(\nabla^2 - \beta_{1j}^2\right)\left(\nabla^2 - \beta_{2j}^2\right)\left(\nabla^2 - \beta_{3j}^2\right)\overline{\phi}_{gj} = 0
\end{cases} \tag{36}
$$

where β_{1j}^2, β_{2j}^2, β_{3j}^2, β_{4j}^2 are eigenvalues. According to operator factorization theory, $\overline{\phi}_{sj} = \overline{\phi}_{sj1} + \overline{\phi}_{sj2} + \overline{\phi}_{sj3}$ and hence, $\left(\nabla^2 - \beta_{1j}^2\right)\overline{\phi}_{sj1} = \left(\nabla^2 - \beta_{2j}^2\right)\overline{\phi}_{sj2} = \left(\nabla^2 - \beta_{3j}^2\right)\overline{\phi}_{sj3} = 0$.

Using separation of variables and setting $\overline{\phi}_{sj1} = R_{sj1}(r)Z_{sj1}(z)$ gives:

$$
\frac{1}{R_{sj1}(r)}\left[\frac{\partial^2 R_{sj1}(r)}{\partial r^2} + \frac{1}{r}\frac{\partial R_{sj1}(r)}{\partial r}\right] + \frac{1}{Z_{sj1}(z)}\frac{\partial^2 Z_{sj1}(z)}{\partial z^2} = \beta_{1j}^2 \tag{37}
$$

Solving Equation (37) yields the general solutions for $R_{sj1}(r)$ and $Z_{sj1}(z)$:

$$
\begin{cases}
R_{sj1}(r) = E_{j1}K_0(q_{j1}r) + F_{j1}I_0(q_{j1}r)\\
Z_{sj1}(z) = G_{j1}e^{g_{j1}z} + H_{j1}e^{-g_{j1}z}
\end{cases} \tag{38}
$$

where $\beta_{1j}^2 = q_{j1}^2 + g_{j1}^2$, $I_0(\cdot)$, $K_0(\cdot)$ denote the modified Bessel functions of the first and second kinds, respectively; E_{j1}, F_{j1}, G_{j1}, H_{j1} are arbitrary constants.

Similarly, by setting $\overline{\phi}_{sj2} = R_{sj2}(r)Z_{sj2}(z)$ and $\overline{\phi}_{sj3} = R_{sj3}(r)Z_{sj3}(z)$ one obtains:

$$
\begin{cases}
R_{sj2}(r) = E_{j2}K_0(q_{j2}r) + F_{j2}I_0(q_{j2}r)\\
Z_{sj2}(z) = G_{j2}e^{g_{j2}z} + H_{j2}e^{-g_{j2}z}\\
R_{sj3}(r) = E_{j3}K_0(q_{j3}r) + F_{j3}I_0(q_{j3}r)\\
Z_{sj3}(z) = G_{j3}e^{g_{j3}z} + H_{j3}e^{-g_{j3}z}
\end{cases} \tag{39}
$$

where $\beta_{2j}^2 = q_{j2}^2 + g_{j2}^2$, $\beta_{3j}^2 = q_{j3}^2 + g_{j3}^2$, E_{j2}, F_{j2}, G_{j2}, H_{j2}, E_{j3}, F_{j3}, G_{j3}, H_{j3} are arbitrary constants.

The remaining scalar potential functions $\overline{\psi}_{sj}$, $\overline{\phi}_{fj}$, $\overline{\psi}_{fj}$, $\overline{\phi}_{gj}$, $\overline{\psi}_{gj}$ can then be obtained using the same procedure, as follows:

$$
\begin{aligned}
\overline{\phi}_{sj} = &\left[E_{j1}\mathrm{K}_0\left(q_{j1}r\right) + F_{j1}\mathrm{I}_0\left(q_{j1}r\right)\right]\left(G_{j1}e^{g_{j1}z} + H_{j1}e^{-g_{j1}z}\right) + \left[E_{j2}\mathrm{K}_0\left(q_{j2}r\right) + F_{j2}\mathrm{I}_0\left(q_{j2}r\right)\right]\cdot\\
&\left(G_{j2}e^{g_{j2}z} + H_{j2}e^{-g_{j2}z}\right) + \left[E_{j3}\mathrm{K}_0\left(q_{j3}r\right) + F_{j3}\mathrm{I}_0\left(q_{j3}r\right)\right]\left(G_{j3}e^{g_{j3}z} + H_{j3}e^{-g_{j3}z}\right)
\end{aligned} \tag{40}
$$

$$
\begin{aligned}
\overline{\phi}_{fj} = &\left[E_{j4}\mathrm{K}_0\left(q_{j1}r\right) + F_{j4}\mathrm{I}_0\left(q_{j1}r\right)\right]\left(G_{j4}e^{g_{j1}z} + H_{j4}e^{-g_{j1}z}\right) + \left[E_{j5}\mathrm{K}_0\left(q_{j2}r\right) + F_{j5}\mathrm{I}_0\left(q_{j2}r\right)\right]\cdot\\
&\left(G_{j5}e^{g_{j2}z} + H_{j5}e^{-g_{j2}z}\right) + \left[E_{j6}\mathrm{K}_0\left(q_{j3}r\right) + F_{j6}\mathrm{I}_0\left(q_{j3}r\right)\right]\left(G_{j6}e^{g_{j3}z} + H_{j6}e^{-g_{j3}z}\right)
\end{aligned} \tag{41}
$$

$$
\begin{aligned}
\overline{\phi}_{gj} = &\left[E_{j7}\mathrm{K}_0\left(q_{j1}r\right) + F_{j7}\mathrm{I}_0\left(q_{j1}r\right)\right]\left(G_{j7}e^{g_{j1}z} + H_{j7}e^{-g_{j1}z}\right) + \left[E_{j8}\mathrm{K}_0\left(q_{j2}r\right) + F_{j8}\mathrm{I}_0\left(q_{j2}r\right)\right]\cdot\\
&\left(G_{j8}e^{g_{j2}z} + H_{j8}e^{-g_{j2}z}\right) + \left[E_{j9}\mathrm{K}_0\left(q_{j3}r\right) + F_{j9}\mathrm{I}_0\left(q_{j3}r\right)\right]\left(G_{j9}e^{g_{j3}z} + H_{j9}e^{-g_{j3}z}\right)
\end{aligned} \tag{42}
$$

$$
\overline{\psi}_{sj} = \left[E_{j10}K_0\left(q_{j4}r\right) + F_{j10}I_0\left(q_{j4}r\right)\right]\left(G_{j10}e^{g_{j4}z} + H_{j10}e^{-g_{j4}z}\right) \tag{43}
$$

$$
\overline{\psi}_{fj} = \left[E_{j11}K_0\left(q_{j4}r\right) + F_{j11}I_0\left(q_{j4}r\right)\right]\left(G_{j11}e^{g_{j4}z} + H_{j11}e^{-g_{j4}z}\right) \tag{44}
$$

$$
\overline{\psi}_{gj} = \left[E_{j12}K_0\left(q_{j4}r\right) + F_{j12}I_0\left(q_{j4}r\right)\right]\left(G_{j12}e^{g_{j4}z} + H_{j12}e^{-g_{j4}z}\right) \tag{45}
$$

where $\beta_{4j}^2 = q_{j4}^2 + g_{j4}^2$, $E_{j4} - E_{j12}$, $F_{j4} - F_{j12}$, $G_{j4} - G_{j12}$ and $H_{j4} - H_{j12}$ are arbitrary constants.

From boundary conditions Equations (17) and (19), we obtain:

$$G_{j1} = -H_{j1}, \ldots, G_{j9} = -H_{j9}, G_{j10} = H_{j10}, \ldots, G_{j12} = H_{j12} \tag{46}$$

$$g_n = g_{j1} = g_{j2} = g_{j3} = g_{j4} = \frac{(2n-1)\pi \mathrm{i}}{2H}, n = 1, 2, 3 \ldots \tag{47}$$

Substituting Equations (40)–(42) into Equation (32), and Equations (43)–(45) into Equation (33) gives:

$$\begin{cases} E_{j4} = d_{j\varepsilon 1} E_{j1}, E_{j5} = d_{j\varepsilon 2} E_{j2}, E_{j6} = d_{j\varepsilon 3} E_{j3}, E_{j11} = d_{j\varepsilon 4} E_{j10} \\ E_{j7} = d_{j\xi 1} E_{j1}, E_{j8} = d_{j\xi 2} E_{j2}, E_{j9} = d_{j\xi 3} E_{j3}, E_{j12} = d_{j\xi 4} E_{j10} \end{cases} \tag{48}$$

$$\begin{cases} F_{j4} = d_{j\varepsilon 1} F_{j1}, F_{j5} = d_{j\varepsilon 2} F_{j2}, F_{j6} = d_{j\varepsilon 3} F_{j3}, F_{j11} = d_{j\varepsilon 4} F_{j10} \\ F_{j7} = d_{j\xi 1} F_{j1}, F_{j8} = d_{j\xi 2} F_{j2}, F_{j9} = d_{j\xi 3} F_{j3}, F_{j12} = d_{j\xi 4} F_{j10} \end{cases} \tag{49}$$

where

$$d_{j\varepsilon n} = \frac{\left(\overline{D}_{3j}\overline{D}_{4j} - \overline{D}_{1j}\overline{D}_{6j}\right)\beta_{kj}^4 + \left(\overline{D}_{1j} b_{3j} - \overline{\rho}_{gj}\delta^2 \overline{D}_{3j} + \overline{\rho}_{fj}\delta^2 \overline{D}_{6j}\right)\beta_{kj}^2 - \overline{\rho}_{fj}\delta^2 b_{3j}}{\left(\overline{D}_{2j}\overline{D}_{6j} - \overline{D}_{3j}\overline{D}_{5j}\right)\beta_{kj}^4 - \left(\overline{D}_{2j} b_{3j} + \overline{D}_{6j} b_{2j}\right)\beta_{kj}^2 + b_{2j} b_{3j}} (k = 1, 2, 3), d_{j\varepsilon 4} = -\frac{\rho_{fj}\delta^2}{b_{2j}}$$

$$d_{j\xi n} = \frac{\left(\overline{D}_{1j}\overline{D}_{5j} - \overline{D}_{2j}\overline{D}_{4j}\right)\beta_{kj}^4 + \left(\overline{D}_{4j} b_{2j} + \overline{\rho}_{gj}\delta^2 \overline{D}_{2j} - \overline{\rho}_{fj}\delta^2 \overline{D}_{5j}\right)\beta_{kj}^2 - \overline{\rho}_{gj}\delta^2 b_{2j}}{\left(\overline{D}_{2j}\overline{D}_{6j} - \overline{D}_{3j}\overline{D}_{5j}\right)\beta_{kj}^4 - \left(\overline{D}_{2j} b_{3j} + \overline{D}_{6j} b_{2j}\right)\beta_{kj}^2 + b_{2j} b_{3j}} (k = 1, 2, 3), d_{j\xi 4} = -\frac{\rho_{gj}\delta^2}{b_{3j}}$$

Equations (40)–(45) are rewritten as the potential functions in the jth zone:

$$\begin{cases} \overline{\phi}_{sj}(r, z) = \sum_{n=1}^{\infty} \sum_{k=1}^{3} \left[A_{jnk} I_0(q_{jk} r) + B_{jnk} K_0(q_{jk} r)\right] \sinh(g_n z) \\ \overline{\phi}_{fj}(r, z) = \sum_{n=1}^{\infty} \sum_{k=1}^{3} d_{j\varepsilon k} \left[A_{jnk} I_0(q_{jk} r) + B_{jnk} K_0(q_{jk} r)\right] \sinh(g_n z) \\ \overline{\phi}_{gj}(r, z) = \sum_{n=1}^{\infty} \sum_{k=1}^{3} d_{j\xi k} \left[A_{jnk} I_0(q_{jk} r) + B_{jnk} K_0(q_{jk} r)\right] \sinh(g_n z) \end{cases} \tag{50}$$

$$\begin{cases} \overline{\psi}_{sj}(r, z) = \sum_{n=1}^{\infty} \left[C_{jn} I_0(q_{j4} r) + D_{jn} K_0(q_{j4} r)\right] \cosh(g_n z) \\ \overline{\psi}_{fj}(r, z) = \sum_{n=1}^{\infty} d_{j\varepsilon 4} \left[C_{jn} I_0(q_{j4} r) + D_{jn} K_0(q_{j4} r)\right] \cosh(g_n z) \\ \overline{\psi}_{gj}(r, z) = \sum_{n=1}^{\infty} d_{j\xi 4} \left[C_{jn} I_0(q_{j4} r) + D_{jn} K_0(q_{j4} r)\right] \cosh(g_n z) \end{cases} \tag{51}$$

where A_{jnk},B_{jnk},C_{jn},D_{jn} are arbitrary constants.

Substituting Equations (50) and (51) into Equations (28)–(30) and using Equation (18), gives:

$$u_{zj} = \begin{cases} \sum_{n=1}^{\infty} \sum_{k=1}^{3} \left[g_n B_{jnk} K_0(q_{jk} r) - q_{j4}^2 D_{jn} K_0(q_{j4} r)\right] \cosh(g_n z) \ \ j = m \\ \sum_{n=1}^{\infty} \left\{ \sum_{k=1}^{3} \ g_n \left[A_{jnk} I_0(q_{jk} r) + B_{jnk} K_0(q_{jk} r)\right] \right. \\ \left. \qquad\qquad -q_{j4}^2 \left[C_{jn} I_0(q_{j4} r) + D_{jn} K_0(q_{j4} r)\right] \right\} \cosh(g_n z) \ j = 1, 2, \cdots, m-1 \end{cases} \tag{52}$$

$$u_{rj} = \begin{cases} \sum_{n=1}^{\infty} \sum_{k=1}^{3} \left[q_{jk} B_{jnk} K_1(q_{jk} r) + g_n q_{j4} D_{jn} K_1(q_{j4} r)\right] \sinh(g_n z) \ j = m \\ \sum_{n=1}^{\infty} \left\{ \sum_{k=1}^{3} -q_{jk} \left[A_{jnk} I_1(q_{jk} r) - B_{jnk} K_1(q_{jk} r)\right] \right. \\ \left. \qquad\qquad -g_n q_{j4} \left[C_{jn} I_1(q_{j4} r) - D_{jn} K_1(q_{j4} r)\right] \right\} \sinh(g_n z) \ j = 1, 2, \cdots, m-1 \end{cases} \tag{53}$$

$$v_{zj} = \begin{cases} \sum_{n=1}^{\infty} \sum_{k=1}^{3} \left[d_{j\varepsilon k} g_n B_{jnk} K_0(q_{jk} r) - d_{j\varepsilon 4} q_{j4}^2 D_{jn} K_0(q_{j4} r)\right] \cosh(g_n z) \ j = m \\ \sum_{n=1}^{\infty} \left\{ \sum_{k=1}^{3} \ d_{j\varepsilon k} g_n \left[A_{jnk} I_0(q_{jk} r) + B_{jnk} K_0(q_{jk} r)\right] \right. \\ \left. \qquad\qquad -d_{j\varepsilon 4} q_{j4}^2 \left[C_{jn} I_0(q_{j4} r) + D_{jn} K_0(q_{j4} r)\right] \right\} \cosh(g_n z) \ j = 1, 2, \cdots, m-1 \end{cases} \tag{54}$$

$$v_{rj} = \begin{cases} \sum_{n=1}^{\infty}\sum_{k=1}^{3}\left[d_{j\varepsilon k}q_{jk}B_{jnk}K_1(q_{jk}r) + d_{j\varepsilon 4}g_n q_{j4}D_{jn}K_1(q_{j4}r)\right]\sinh(g_n z)\ j = m \\ \sum_{n=1}^{\infty}\left\{\begin{array}{l}\sum_{k=1}^{3} -d_{j\varepsilon k}q_{jk}\left[A_{jnk}I_1(q_{jk}r) - B_{jnk}K_1(q_{jk}r)\right] \\ -d_{j\varepsilon 4}g_n q_{j4}\left[C_{jn}I_1(q_{j4}r) - D_{jn}K_1(q_{j4}r)\right]\end{array}\right\}\sinh(g_n z)\ \ j = 1,2,\cdots,m-1 \end{cases} \tag{55}$$

$$w_{zj} = \begin{cases} \sum_{n=1}^{\infty}\sum_{k=1}^{3}\left[d_{j\xi k}g_n B_{jnk}K_0(q_{jk}r) - d_{j\xi 4}q_{j4}^2 D_{jn}K_0(q_{j4}r)\right]\cosh(g_n z)\ j = m \\ \sum_{n=1}^{\infty}\left\{\begin{array}{l}\sum_{k=1}^{3} d_{j\xi k}g_n\left[A_{jnk}I_0(q_{jk}r) + B_{jnk}K_0(q_{jk}r)\right] \\ -d_{j\xi 4}q_{j4}^2\left[C_{jn}I_0(q_{j4}r) + D_{jn}K_0(q_{j4}r)\right]\end{array}\right\}\cosh(g_n z)\ \ j = 1,2,\cdots,m-1 \end{cases} \tag{56}$$

$$w_{rj} = \begin{cases} \sum_{n=1}^{\infty}\sum_{k=1}^{3}\left[d_{j\xi k}q_{jk}B_{jnk}K_1(q_{jk}r) + d_{j\xi 4}g_n q_{j4}D_{jn}K_1(q_{j4}r)\right]\sinh(g_n z)\ j = m \\ \sum_{n=1}^{\infty}\left\{\begin{array}{l}\sum_{k=1}^{3} -d_{j\xi k}q_{jk}\left[A_{jnk}I_1(q_{jk}r) - B_{jnk}K_1(q_{jk}r)\right] \\ -d_{j\xi 4}g_n q_{j4}\left[C_{jn}I_1(q_{j4}r) - D_{jn}K_1(q_{j4}r)\right]\end{array}\right\}\sinh(g_n z)\ \ j = 1,2,\cdots,m-1 \end{cases} \tag{57}$$

Substituting Equations (52)–(57) into Equations (12)–(15) gives:

$$\tau_{zrj}(r,z) = \begin{cases} \sum_{n=1}^{\infty}\sum_{k=1}^{3}\left[2G_{sj}q_{jk}g_n B_{jnk}K_1(q_{jk}r) + G_{sj}(g_n^2 - q_{j4}^2)q_{j4}D_{jn}K_1(q_{j4}r)\right]\cosh(g_n z)\ j = m \\ \sum_{n=1}^{\infty}\left\{\begin{array}{l}\sum_{k=1}^{3} -2G_{sj}q_{jk}g_n\left[A_{jnk}I_1(q_{jk}r) - B_{jnk}K_1(q_{jk}r)\right] \\ -G_{sj}(g_n^2 - q_{j4}^2)q_{j4}\left[C_{jn}I_1(q_{j4}r) - D_{jn}K_1(q_{j4}r)\right]\end{array}\right\}\cosh(g_n z)\ \ j = 1,2,\cdots,m-1 \end{cases} \tag{58}$$

$$\sigma_{zj}(r,z) = \sum_{n=1}^{\infty}\left\{\begin{array}{l}\sum_{k=1}^{3} \left[\lambda_{cj}\beta_{kj}^2 + 2G_{sj}g_n^2 + a(\gamma D_{fjk} + (1-\gamma)D_{gjk})\beta_{kj}^2\right] \\ \cdot\left[A_{jnk}I_0(q_{jk}r) + B_{jnk}K_0(q_{jk}r)\right] \\ -2G_{sj}g_n^2 q_{j4}^2\left[C_{jn}I_0(q_{j4}r) + D_{jn}K_0(q_{j4}r)\right])\end{array}\right\}\cosh(g_n z) \tag{59}$$

$$p_{fj}(r,z) = -\sum_{n=1}^{\infty}\sum_{k=1}^{3} D_{fjk}\beta_{kj}^2\left[A_{jnk}I_0(q_{jk}r) + B_{jnk}K_0(q_{jk}r)\right]\sinh(g_n z) \tag{60}$$

$$p_{gj}(r,z) = -\sum_{n=1}^{\infty}\sum_{k=1}^{3} D_{gjk}\beta_{kj}^2\left[A_{jnk}I_0(q_{jk}r) + B_{jnk}K_0(q_{jk}r)\right]\sinh(g_n z) \tag{61}$$

where $D_{fjk} = D_{1j} + D_{2j}d_{j\varepsilon k} + D_{3j}d_{j\xi k}$,$D_{gjk} = D_{4j} + D_{5j}d_{j\varepsilon k} + D_{6j}d_{j\xi k}$.

From Equations (52)–(57), the coefficient vector in the undisturbed region is:

$$\Theta_{mn} = [0, B_{mn1}, 0, B_{mn2}, 0, B_{mn3}, 0, D_{mn}]^T \tag{62}$$

The coefficient vector in the jth zone for the nth order is:

$$\Theta_{jn} = \left[A_{jn1}, B_{jn1}, A_{jn2}, B_{jn2}, A_{jn3}, B_{jn3}, C_{jn}, D_{jn}\right]^T \tag{63}$$

At a radial coordinate r, the eight state variables (u_z, u_r, v_r, w_r, τ_{zr}, σ_z, p_f, p_a) can be represented as a linear combination of the components of Θ_{jn}. Based on Equations (52), (53), (55), (57), and (58)–(61), the eight rows of the matrix $M_{jn}(r)$ are associated with the corresponding eight state variables, respectively. Each row contains eight coefficients corresponding to the eight components of Θ_{jn}.

The interface matrix of order j in the nth layer at radius r, $M_{jn}(r)$, can be written uniformly as:

$$M_{jn}(r) = \begin{bmatrix} g_n I_0(q_{j1}r) & g_n K_0(q_{j1}r) & g_n I_0(q_{j2}r) & g_n K_0(q_{j2}r) \\ -q_{j1} I_1(q_{j1}r) & q_{j1} K_1(q_{j1}r) & -q_{j2} I_1(q_{j2}r) & q_{j2} K_1(q_{j2}r) \\ -d_{j\varepsilon 1} q_{j1} I_1(q_{j1}r) & d_{j\varepsilon 1} q_{j1} K_1(q_{j1}r) & -d_{j\varepsilon 2} q_{j2} I_1(q_{j2}r) & d_{j\varepsilon 2} q_{j2} K_1(q_{j2}r) \\ -d_{j\xi 1} q_{j1} I_1(q_{j1}r) & d_{j\xi 1} q_{j1} K_1(q_{j1}r) & -d_{j\xi 2} q_{j2} I_1(q_{j2}r) & d_{j\xi 2} q_{j2} K_1(q_{j2}r) \\ -2G_{sj} g_n q_{j1} I_1(q_{j1}r) & 2G_{sj} g_n q_{j1} K_1(q_{j1}r) & -2G_{sj} g_n q_{j2} I_1(q_{j2}r) & 2G_{sj} g_n q_{j2} K_1(q_{j2}r) \\ Q_{j1} I_0(q_{j1}r) & Q_{j1} K_0(q_{j1}r) & Q_{j2} I_0(q_{j2}r) & Q_{j2} K_0(q_{j2}r) \\ -D_{fj1} \beta_{1j}^2 I_0(q_{j1}r) & -D_{fj1} \beta_{1j}^2 K_0(q_{j1}r) & -D_{fj2} \beta_{2j}^2 I_0(q_{j2}r) & -D_{fj2} \beta_{2j}^2 K_0(q_{j2}r) \\ -D_{gj1} \beta_{1j}^2 I_0(q_{j1}r) & -D_{gj1} \beta_{1j}^2 K_0(q_{j1}r) & -D_{gj2} \beta_{2j}^2 I_0(q_{j2}r) & -D_{gj2} \beta_{2j}^2 I_0(q_{j2}r) \end{bmatrix}$$

$$\begin{bmatrix} g_n I_0(q_{j3}r) & g_n K_0(q_{j3}r) & -q_{j4}^2 I_0(q_{j4}r) & -q_{j4}^2 K_0(q_{j4}r) \\ -q_{j3} I_1(q_{j3}r) & q_{j3} K_1(q_{j3}r) & -g_n q_{j4} I_1(q_{j4}r) & g_n q_{j4} K_1(q_{j4}r) \\ -d_{j\varepsilon 3} q_{j3} I_1(q_{j3}r) & d_{j\varepsilon 3} q_{j3} K_1(q_{j3}r) & -d_{j\varepsilon 4} g_n q_{j4} I_1(q_{j4}r) & d_{j\varepsilon 4} g_n q_{j4} K_1(q_{j4}r) \\ -d_{j\xi 3} q_{j3} I_1(q_{j3}r) & d_{j\xi 3} q_{j3} K_1(q_{j3}r) & -d_{j\varepsilon 4} g_n q_{j4} I_1(q_{j4}r) & d_{j\varepsilon 4} g_n q_{j4} K_1(q_{j4}r) \\ -2G_{sj} g_n q_{j3} I_1(q_{j3}r) & 2G_{sj} g_n q_{j3} K_1(q_{j3}r) & -G_{sj}(g_n^2 + q_{j4}^2) q_{j4} I_1(q_{j4}r) & G_{sj}(g_n^2 + q_{j4}^2) q_{j4} K_1(q_{j4}r) \\ Q_{j3} I_0(q_{j3}r) & Q_{j3} K_0(q_{j3}r) & -2G_{sj} g_n^2 q_{j4}^2 I_0(q_{j4}r) & -2G_{sj} g_n^2 q_{j4}^2 K_0(q_{j4}r) \\ -D_{fj3} \beta_{3j}^2 I_0(q_{j3}r) & -D_{fj3} \beta_{3j}^2 K_0(q_{j3}r) & 0 & 0 \\ -D_{gj3} \beta_{3j}^2 I_0(q_{j3}r) & -D_{gj3} \beta_{3j}^2 K_0(q_{j3}r) & 0 & 0 \end{bmatrix} \quad (64)$$

where $Q_{jk} = \lambda_j \beta_{kj}^2 + 2G_{sj} g_n^2 + a(\gamma D_{fjk} + (1-\gamma) D_{gjk}) \beta_{kj}^2$.

From Equations (20)–(22), we have:

$$M_{jn}(r_{j+1}) \Theta_{jn} = M_{(j+1)n}(r_{j+1}) \Theta_{(j+1)n} \quad (65)$$

It can be obtained from Equation (65) that

$$\Theta_{(j+1)n} = T_{jn} \Theta_{jn} \quad (66)$$

where the transfer matrix is $T_{jn} = \left[M_{(j+1)n}(r_{j+1}) \right]^{-1} M_{jn}(r_{j+1})$.

By transferring zone by zone, the innermost coefficient vector can be related to the outermost coefficient vector:

$$\Theta_{1n} = T_{1n}^{-1} T_{2n}^{-1} \cdots T_{(m-1)n}^{-1} \Theta_{mn} = S_n \Theta_{mn} \quad (67)$$

where S_n is the total transfer matrix.

Substituting Equations (53), (55), (57) and (67) into Equation (25) we can be obtained:

$$\begin{cases} q_{m1} K_1(q_{m1}r) B_{mn1} + q_{m2} K_1(q_{m2}r) B_{mn2} + q_{m3} K_1(q_{m3}r) B_{mn3} + g_n q_{m4} K_1(q_{m4}r) B_{mn4} = 0 \\ d_{m\varepsilon 1} q_{m1} K_1(q_{m1}r) B_{mn1} + d_{m\varepsilon 2} q_{m2} K_1(q_{m2}r) B_{mn2} + d_{m\varepsilon 3} q_{m3} K_1(q_{m3}r) B_{mn3} + d_{m\varepsilon 4} g_n q_{m4} K_1(q_{m4}r) B_{mn4} = 0 \\ d_{m\xi 1} q_{m1} K_1(q_{m1}r) B_{mn1} + d_{m\xi 2} q_{m2} K_1(q_{m2}r) B_{mn2} + d_{m\xi 3} q_{m3} K_1(q_{m3}r) B_{mn3} + d_{m\xi 4} g_n q_{m4} K_1(q_{m4}r) B_{mn4} = 0 \end{cases} \quad (68)$$

According to Equation (68), the relationship between the coefficients and B_{mn1} can be obtained as follows:

$$B_{mn2} = \eta_{n2} B_{mn1}, B_{mn3} = \eta_{n3} B_{mn1}, D_{mn} = \eta_{n4} B_{mn1} \quad (69)$$

where $\eta_{n2} = \frac{|N_2|}{|N_1|}$; $\eta_{n3} = \frac{|N_3|}{|N_1|}$; $\eta_{n4} = \frac{|N_4|}{|N_1|}$;

$$|N_1| = \begin{vmatrix} q_{m2} K_1(q_{m2}r) & q_{m3} K_1(q_{m3}r) & g_n q_{m4} K_1(q_{m4}r) \\ d_{m\varepsilon 2} q_{m2} K_1(q_{m2}r) & d_{m\varepsilon 3} q_{m3} K_1(q_{m3}r) & d_{m\varepsilon 4} g_n q_{m4} K_1(q_{m4}r) \\ d_{m\xi 2} q_{m2} K_1(q_{m2}r) & d_{m\xi 3} q_{m3} K_1(q_{m3}r) & d_{m\xi 4} g_n q_{m4} K_1(q_{m4}r) \end{vmatrix};$$

$$|N_2| = \begin{vmatrix} -q_{m1} K_1(q_{m1}r) & q_{m3} K_1(q_{m3}r) & g_n q_{m4} K_1(q_{m4}r) \\ -d_{m\varepsilon 1} q_{m1} K_1(q_{m1}r) & d_{m\varepsilon 3} q_{m3} K_1(q_{m3}r) & d_{m\varepsilon 4} g_n q_{m4} K_1(q_{m4}r) \\ -d_{m\xi 1} q_{m1} K_1(q_{m1}r) & d_{m\xi 3} q_{m3} K_1(q_{m3}r) & d_{m\xi 4} g_n q_{m4} K_1(q_{m4}r) \end{vmatrix};$$

$$|N_3| = \begin{vmatrix} q_{m2}K_1(q_{m2}r) - q_{m1}K_1(q_{m1}r)g_n q_{m4}K_1(q_{m4}r) \\ d_{m\varepsilon 2}q_{m2}K_1(q_{m2}r) - d_{m\varepsilon 1}q_{m1}K_1(q_{m1}r)d_{m\varepsilon 4}g_n q_{m4}K_1(q_{m4}r) \\ d_{m\xi 2}q_{m2}K_1(q_{m2}r) - d_{m\xi 1}q_{m1}K_1(q_{m1}r)d_{m\xi 4}g_n q_{m4}K_1(q_{m4}r) \end{vmatrix};$$

$$|N_4| = \begin{vmatrix} q_{m2}K_1(q_{m2}r)q_{m3}K_1(q_{m3}r) - q_{m1}K_1(q_{m1}r) \\ d_{m\varepsilon 2}q_{m2}K_1(q_{m2}r)d_{m\varepsilon 3}d_{m\varepsilon 3}q_{m3}K_1(q_{m3}r) - d_{m\varepsilon 1}q_{m1}K_1(q_{m1}r) \\ d_{m\xi 2}q_{m2}K_1(q_{m2}r)d_{m\xi 3}d_{m\xi 3}q_{m3}K_1(q_{m3}r) - d_{m\xi 1}q_{m1}K_1(q_{m1}r) \end{vmatrix}.$$

Thus, the relationship between the coefficients in zone 1 and B_{mn1} is obtained as:

$$\Theta_{1n} = S_n[0, 1, 0, \eta_{n2}, 0, \eta_{n3}, 0, \eta_{n4}]B_{mn1} = \chi_n B_{mn1} \tag{70}$$

3.2. Solution of the Pile Governing Equation

Substituting Equation (27) into Equation (16) gives:

$$v_p^2\left(1 + \frac{\delta_p i\omega}{E_p}\right)\frac{d^2u_p}{dz^2} + \omega^2 u_p - \frac{2\pi r_1 G_{s1}}{\rho_p A_p}\sum_{n=1}^{\infty}\Omega_{2n}B_{mn1}\cosh(g_n z) = 0 \tag{71}$$

where $\Omega_{2n} = \sum_{k=1}^{3} -2g_n q_{1k}\chi_{nk}^{(2k)}K_1(q_{1k}r_1) - (g_n^2 - q_{14}^2)q_{14}\chi_{n4}^{(8)}K_1(q_{14}r_1)$; $v_p = \sqrt{E_p/\rho_p}$ is the longitudinal-wave velocity of the pile.

The solution of Equation (71) is given by:

$$u_p = a_1 e^{\frac{\overline{\lambda}z}{H}} + a_2 e^{-\frac{\overline{\lambda}z}{H}} + \sum_{n=1}^{\infty} I_n \cosh(g_n z) \tag{72}$$

where a_1 and a_2 are arbitrary constants; $\overline{\lambda} = \sqrt{\frac{-\omega^2 T_c^2}{1+\delta_p i\omega/E_p}}$, $T_c = \frac{H}{v_p}$ is the travel time of the elastic wave from the pile head to the pile tip, and I_n is a particular solution of Equation (72). $I_n = -\frac{2\pi r_1 G_{s1}}{\rho_p A_p} \cdot \frac{\Omega_{2n}B_{mn1}}{\omega^2 - \frac{H^2 g_n^2 \omega^2}{\overline{\lambda}^2}}$.

According to Equation (26), we obtain:

$$a_1 e^{\frac{\overline{\lambda}}{H}z} + a_2 e^{-\frac{\overline{\lambda}}{H}z} + \sum_{n=1}^{\infty} I_n \cosh(g_n z) = \sum_{n=1}^{\infty}\Omega_{1n}B_{mn1}cosh(g_n z) \tag{73}$$

where $\Omega_{1n} = \sum_{k=1}^{3} g_n\chi_{nk}^{(2k)}K_0(q_{1k}r_1) - q_{14}^2\chi_{n4}^{(8)}K_0(q_{14}r_1)$.

Multiplying both sides of Equation (73) by $\cosh(g_n z)dz$, and integrating over the domain $[0, H]$, the expression for B_{mn1} can be obtained as

$$B_{mn1} = \frac{1}{T_n L_n}\int_0^H \left(a_1 e^{\frac{\overline{\lambda}}{H}z} + a_2 e^{-\frac{\overline{\lambda}}{H}z}\right)\cosh(g_n z)dz \tag{74}$$

where $T_n = \Omega_{1n} + \frac{2\pi r_1 G_{s1}\Omega_{2n}}{\rho_p A_p(\omega^2 - \frac{H^2 g_n^2 \omega^2}{\overline{\lambda}^2})}$, $L_n = \int_0^H \cosh^2(g_n z)dz$.

Substituting Equation (74) into Equation (72), the displacement response amplitude of the pile is obtained as follows:

$$u_p = a_1\left[e^{\overline{\lambda}\overline{z}} + \sum_{n=1}^{\infty}(\gamma'_n + \gamma''_n)\cosh(\overline{g_n z})\right] + a_2\left[e^{-\overline{\lambda}\overline{z}} + \sum_{n=1}^{\infty}(\gamma'_n - \gamma''_n)\cosh(\overline{g_n z})\right] \tag{75}$$

where

$$\gamma'_n = \gamma_n\left[\frac{\sinh(\overline{\lambda} - \overline{g_n})}{\overline{\lambda} - \overline{g_n}} + \frac{\sinh(\overline{\lambda} + \overline{g_n})}{\overline{\lambda} + \overline{g_n}}\right] \tag{76}$$

$$\gamma''_n = \gamma_n\left[\frac{\cosh(\overline{\lambda} + \overline{g_n}) - 1}{\overline{\lambda} + \overline{g_n}} + \frac{\cosh(\overline{\lambda} - \overline{g_n}) - 1}{\overline{\lambda} - \overline{g_n}}\right] \tag{77}$$

$$\gamma_n = -\frac{\overline{G_{s1}}\overline{\Omega}_{2n}}{\overline{r_1}(\overline{\omega}^2 - \overline{g_n}^2\overline{\omega}^2/\overline{\lambda}^2)\overline{T_n}\overline{L_n}} \tag{78}$$

$$\overline{T}_n = \overline{\Omega}_{1n} + \frac{2\overline{G}_{s1}\overline{\Omega}_{2n}}{\overline{r_1}(\overline{\omega}^2 - \overline{g_n}^2\overline{\omega}^2/\overline{\lambda}^2)} \tag{79}$$

in which $\overline{L_n} = \frac{1}{H}L_n = \int_0^1 \cosh^2(\overline{g_n}\overline{z})d\overline{z}$; $\overline{\Omega}_{1n} = \sum_{k=1}^{3} \overline{g}_n\chi_{nk}^{(2k)}K_0(\overline{q}_{1k}\overline{r}_1) - \overline{q}_{14}^2\chi_{n4}^{(8)}K_0(\overline{q}_{14}\overline{r}_1)$; $\overline{r_1} = r_1/H$; $\overline{\Omega}_{2n} = \sum_{k=1}^{3} -2\overline{g}_n\overline{q}_{1k}\boldsymbol{\chi}_{nk}^{(2k)}K_1(\overline{q}_{1k}\overline{r}_1) - (\overline{g}_n^2 + \overline{q}_{14}^2)\overline{q}_{14}\boldsymbol{\chi}_{n4}^{(8)}K_1(\overline{q}_{14}\overline{r}_1)$ $\overline{z} = z/H$; $\overline{G_{s1}} = G_{s1}/E_p$; $\overline{\omega} = \omega T_c$; $\overline{q_{1k}} = q_{1k}H, k = 1, 2, 3, 4$ and $\overline{g_n} = g_nH$ are dimensionless coefficients.

The dimensionless expressions of Equations (23) and (24) can be respectively written as

$$\left(1 + \frac{\delta_p i\omega}{E_p}\right)\frac{du_p(\overline{z})}{d\overline{z}}\bigg|_{\overline{z}=0} = -\frac{P_0H}{E_pA_p} \tag{80}$$

$$u_p(\overline{z})\big|_{\overline{z}=1} = 0 \tag{81}$$

The substitution of Equation (75) into Equations (80) and (81) results in

$$a_1 = \frac{-P_0H\varsigma}{\overline{\lambda}(\varsigma - 1)(E_pA_p + A_p\delta_p i\omega)} \tag{82}$$

$$a_2 = \frac{-P_0H}{\overline{\lambda}(\varsigma - 1)(E_pA_p + A_p\delta_p i\omega)} \tag{83}$$

where $\varsigma = -\frac{e^{-\overline{\lambda}} + \sum_{n=1}^{\infty}(\gamma'_n - \gamma''_n)\cosh(\overline{g_n})}{e^{\overline{\lambda}} + \sum_{n=1}^{\infty}(\gamma'_n + \gamma''_n)\cosh(\overline{g_n})}$.

The complex impedance function of the pile-head displacement is expressed as follows:

$$Z_p = \frac{P_0}{u_p(\overline{z})\big|_{\overline{z}=0}} = \frac{E_pA_p}{H}Z'_p \tag{84}$$

where Z'_p is the dimensionless displacement complex impedance of Z_p, expressed as:

$$Z'_p = -\left(1 + \frac{\delta_{\mathrm{p}}\mathrm{i}\omega}{E_{\mathrm{p}}}\right)\frac{\overline{\lambda}(\varsigma - 1)}{\varsigma\left[1 + \sum_{n=1}^{\infty}(\gamma'_n + \gamma''_n)\right] + \left[1 + \sum_{n=1}^{\infty}(\gamma'_n - \gamma''_n)\right]} \tag{85}$$

Z'_p can be further written as:

$$Z'_p = \mathrm{Re}(Z'_p) + \mathrm{iIm}(Z'_p) \tag{86}$$

where $\mathrm{Re}(Z'_p)$ and $\mathrm{Im}(Z'_p)$ represent the dynamic stiffness and damping coefficients.

4. Validation and Parametric Analysis

The reliability and precision of the proposed analytical framework are first verified through comparison with results reported in earlier studies. A systematic parametric investigation is then performed to examine how pile–soil characteristics and construction-related disturbances affect the pile's vertical dynamic behavior. Unless stated otherwise, the material and geometric parameters assigned to the pile and adjacent soil are kept constant throughout the following analyses. $H = 10$ m, $r_p = 0.5$ m, $v_p = 3600$ m/s, $\delta_p = 10{,}000$ N · s/m^2, $\rho_p = 2500$ kg/m^3, $\rho_s = 2700$ kg/m^3, $\rho_f = 1000$ kg/m^3, $\rho_g = 1.29$ kg/m^3, $K_s = 36$ GPa, $K_f = 2.0$ GPa, $K_g = 145$ kPa, $\eta_f = 1.0 \times 10^{-3}$ Pa · s, $\eta_g = 1.0 \times 10^{-3}$ Pa · s, $n = 0.4$, $S_{wo} = 0.05$, $K_d = 1.0 \times 10^{-12}$ m^2, $\varphi = 20°$, $m_1 = 0.5$, $d = 2$, $\alpha = 1.0 \times 10^{-4}$ Pa^{-1}, $S_r = 0.6$. Based on the study by Xu and Wei [54], the relationship between the shear modulus and the degree of saturation

for unsaturated soils can be established as: $G_{sj} = \mu + \frac{2200}{\alpha} \ln\left(\sqrt{S_e^{-2} - 1} + S_e^{-1}\right) \tan\varphi'$ where μ is the shear modulus of the saturated soil and is assigned as 20 MPa. Subsequently, the shear modulus of the innermost unsaturated soil layer is calculated to be $G_{s1} = 23$ MPa. The disturbance zone extends over $r_d = 2r_p$, and the shear modulus of the soil in this zone is simplified as varying linearly in the radial direction; the degree of disturbance is defined as $x = G_{s1}/G_{sm}$.

The linear profile is an idealized modeling assumption rather than a distribution fitted to measurements in this study. It provides a simple transition between disturbed and undisturbed soil, allowing disturbance intensity and extent to be examined separately.

4.1. Validation of the Solution

The soil domain around the pile is discretized into m concentric annular regions in the radial direction. To verify the numerical adequacy of this discretization, a convergence analysis is first carried out to determine the influence of m within the disturbed zone on the computed complex impedance at the pile head. Figures 2 and 3 present the corresponding impedance responses obtained using different radial discretization schemes. For both softened and hardened soil conditions, the results approach stable values progressively as the number of annular regions increases. In the present analysis, convergence is effectively achieved at $m = 200$, beyond which further refinement produces only insignificant changes in the pile-head impedance. Accordingly, $m = 200$ is adopted in all subsequent calculations.

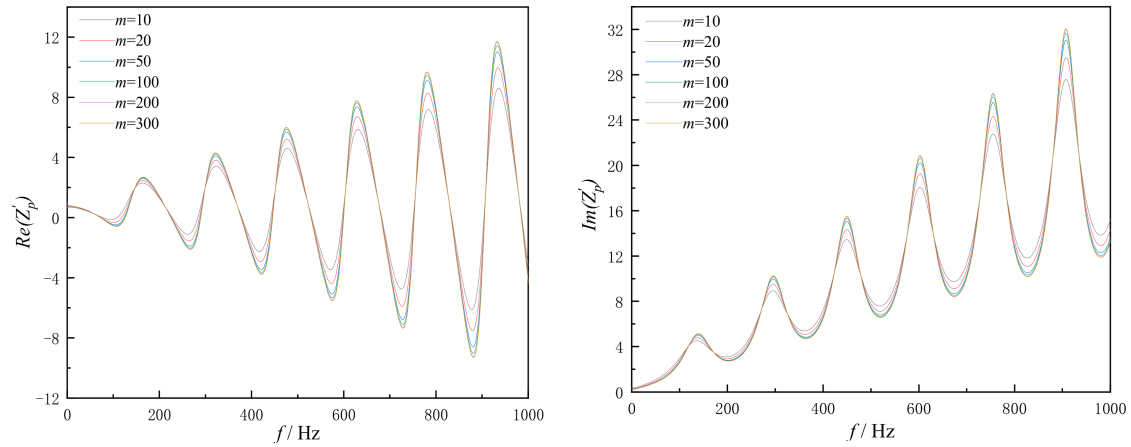


Figure 2. Effect of m under soil softening condition.

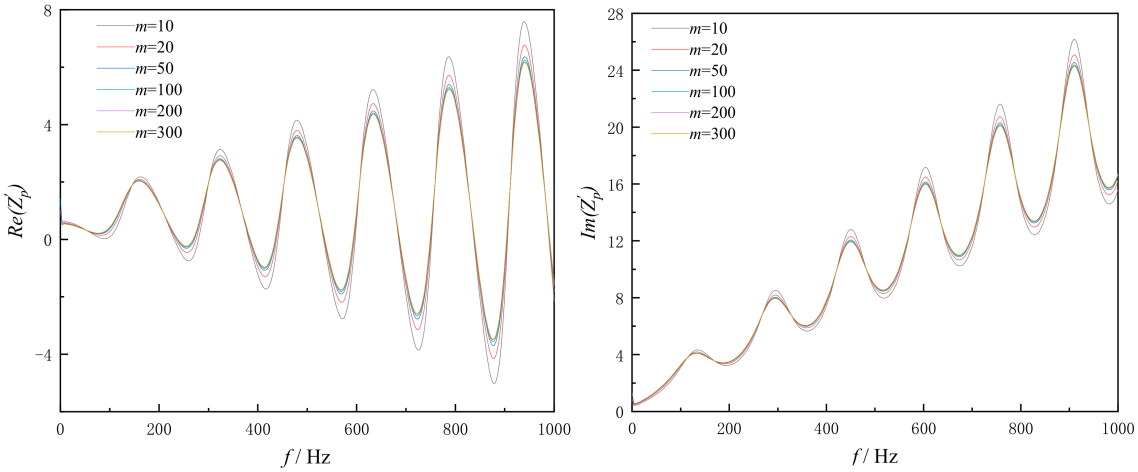


Figure 3. Effect of m under soil hardening condition.

In the subsequent parametric analysis, unless otherwise required, m is set to 200. In addition, $x = 0.6$ and $x = 1.4$ are used to represent soil softening and soil hardening, respectively. For more complex conditions, the number of annular zones m and the degree of soil softening or hardening, x, should be redefined accordingly.

When the parameter x is assigned a value of 1, the developed formulation can be simplified to describe the behavior of a pile embedded in homogeneous unsaturated soil. The resulting expression is subsequently validated against the analytical results presented by Shan et al., with both solutions further considering the limiting condition of an end-bearing pile. As illustrated in Figure 4, the two approaches exhibit a high degree of consistency, demonstrating the accuracy and credibility of the proposed analytical framework.

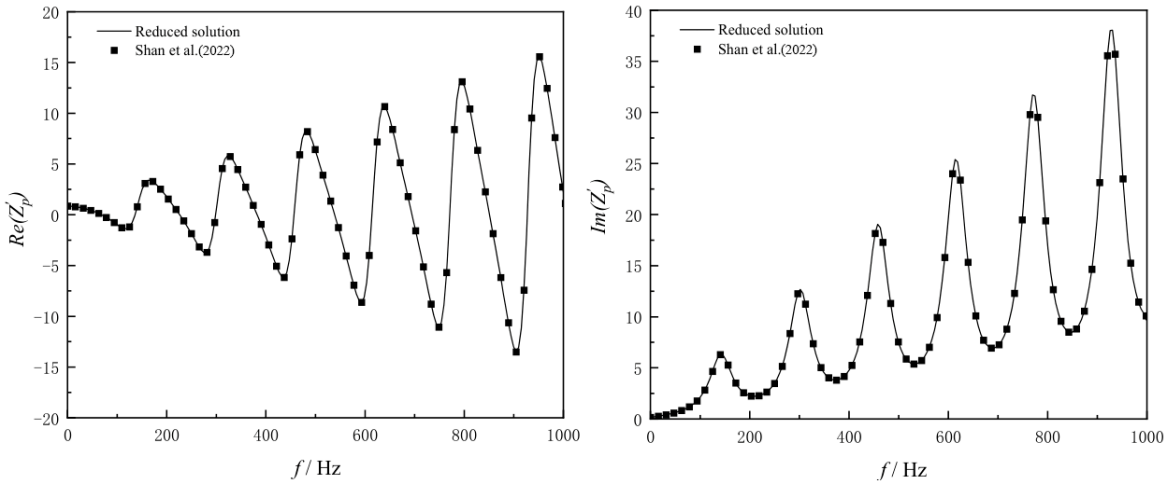


Figure 4. Comparison with Shan et al. [32]

When S_r is assigned a value of 0.999 and x is assigned a value of 1, the developed analytical solution can be reduced to describe the behavior of a pile embedded in homogeneous saturated soil. With all parameter values taken to be identical to those specified in Cui et al., the resulting reduced solution is compared with the corresponding solution for an end-bearing pile presented therein, as illustrated in Figure 5. The results show that the two solutions are in complete agreement.

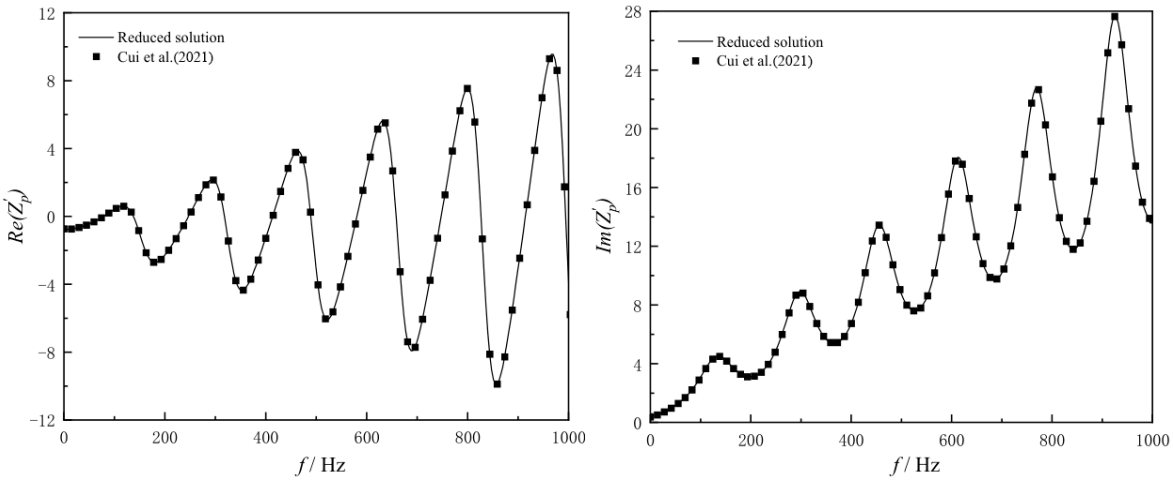


Figure 5. Comparison with Cui et al. [19]

4.2. Parametric Analysis

This section focuses on the influence of construction-induced disturbances in combination with various pile–soil parameters on the complex impedance characteristics at the pile head.

(1) Effect of soil saturation

Figure 6 illustrates the pile-head complex impedance responses corresponding to different degrees of soil saturation. With increasing excitation frequency, the resonance peaks of both the dynamic stiffness and damping components become progressively more pronounced. Relative to the softened-soil case, soil hardening leads to lower resonance magnitudes for both impedance components. The observed trend is mainly associated with the reduction in soil shear modulus as saturation increases, which intensifies the resonance response under both softening and hardening conditions. This saturation effect is particularly evident at higher frequencies. In contrast, only minor shifts are observed in the resonance frequencies, suggesting that saturation predominantly governs the response amplitude while exerting little influence on its characteristic frequency. Within the adopted constitutive relationship, increasing saturation reduces the soil shear modulus and consequently increases the relative stiffness of the pile with respect to the surrounding soil. This change modifies the shaft restraint and the transfer of vibration energy into the soil, contributing to the more pronounced oscillatory impedance peaks. The limited changes in peak frequencies suggest that, within the investigated parameter range, these frequencies remain primarily controlled by the pile properties and the imposed boundary conditions.

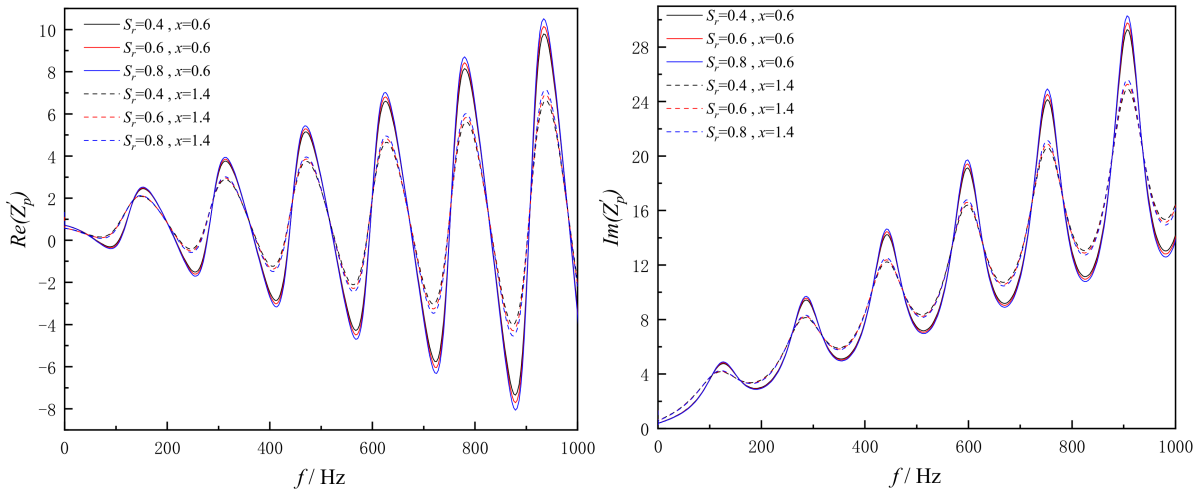


Figure 6. Effect of soil saturation on pile complex impedance.

(2) Effect of construction disturbance at different degrees of saturation

Figures 7 and 8 depict the effects of disturbed-zone thickness on the complex impedance at the pile head for different degrees of saturation. As shown in Figure 7, expansion of the softened soil zone progressively increases the magnitudes of both stiffness and damping responses, with the effect becoming especially pronounced at relatively high excitation frequencies. Moreover, increasing the saturation degree from 0.4 to 0.8 intensifies the influence of the softened-region thickness, indicating that wetter soil conditions make the pile response more sensitive to the spatial extent of softening. By contrast, Figure 8. shows that widening the hardened soil zone suppresses the amplitudes of both impedance components. This dependence on hardened-zone thickness likewise becomes stronger as saturation increases.

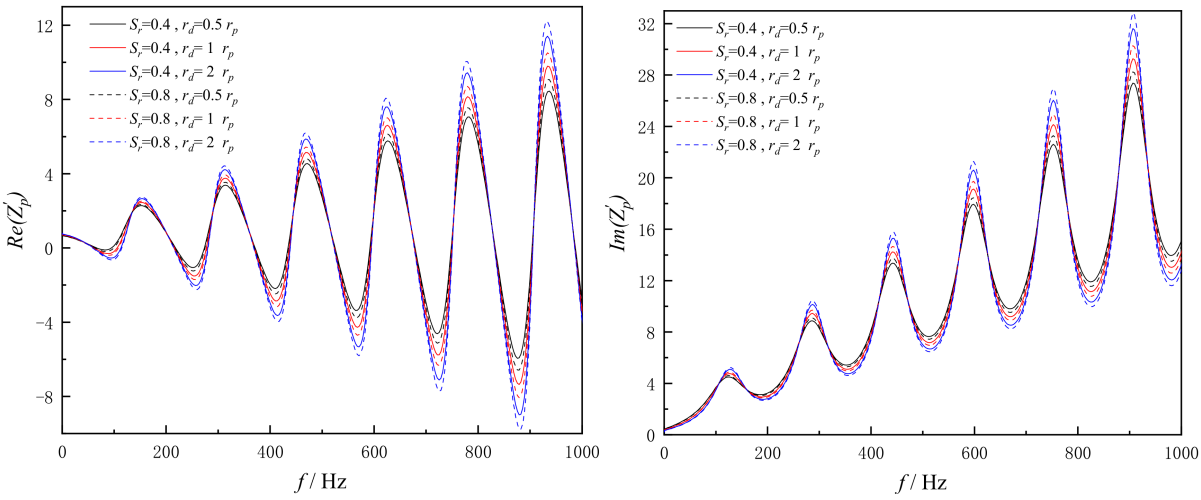


Figure 7. Effects of soil saturation and softening range on pile complex impedance.

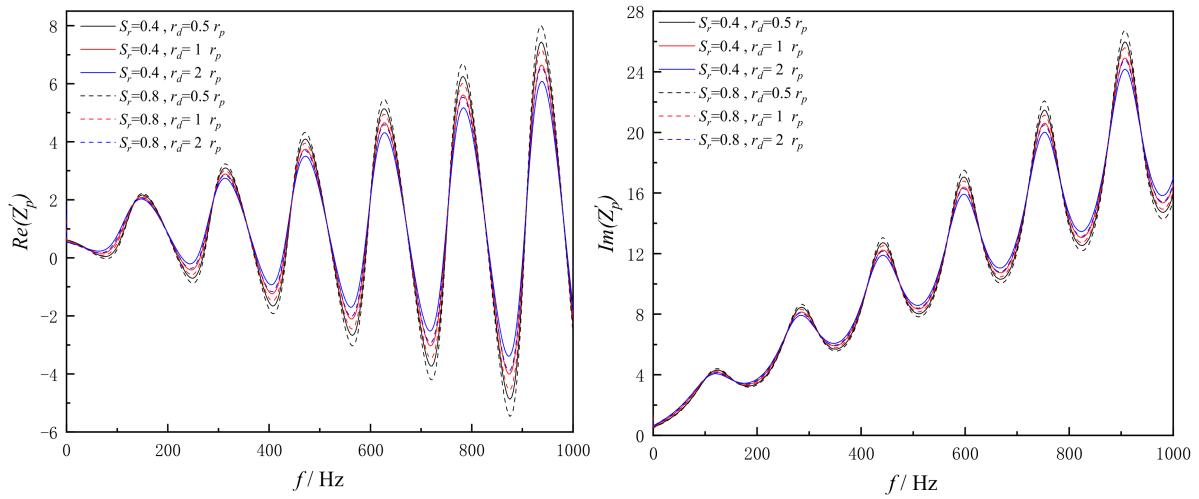


Figure 8. Effects of soil saturation and hardening range on pile complex impedance.

Figures 9 and 10 further illustrate how disturbance intensity affects pile-head impedance at different saturation levels. According to Figure 9, a greater degree of soil softening enhances both stiffness- and damping-related response amplitudes, and this tendency is particularly marked when the saturation degree reaches 0.8. The opposite trend is observed for soil hardening: Figure 10 indicates that stronger hardening leads to progressively smaller impedance amplitudes. The reduction becomes more substantial at higher saturation levels, highlighting the coupled effects of disturbance intensity and soil saturation on the vertical dynamic response of the pile–soil system. Construction disturbance changes both the local soil restraint and the radial distribution of wave impedance. Softening reduces the near-pile shear stiffness, whereas hardening increases it; both conditions modify wave transmission and reflection through the disturbed region. Changing the disturbance extent also changes the wave travel path within this region. These effects jointly contribute to the frequency-dependent differences between the impedance curves. Accordingly, the larger oscillatory peaks observed under softening should be distinguished from an increase in the low-frequency supporting stiffness.

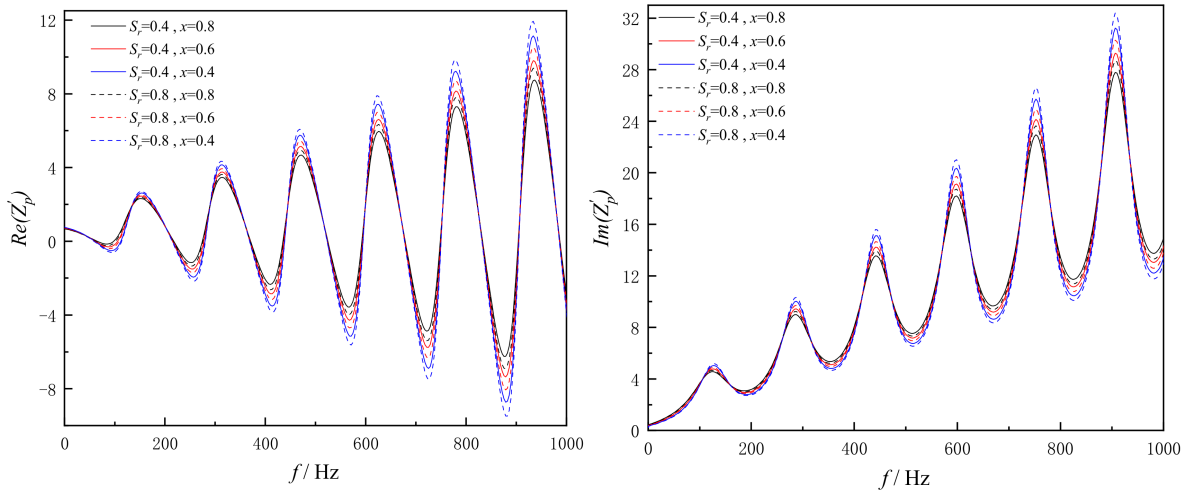


Figure 9. Effects of soil saturation and softening degree on pile complex impedance.

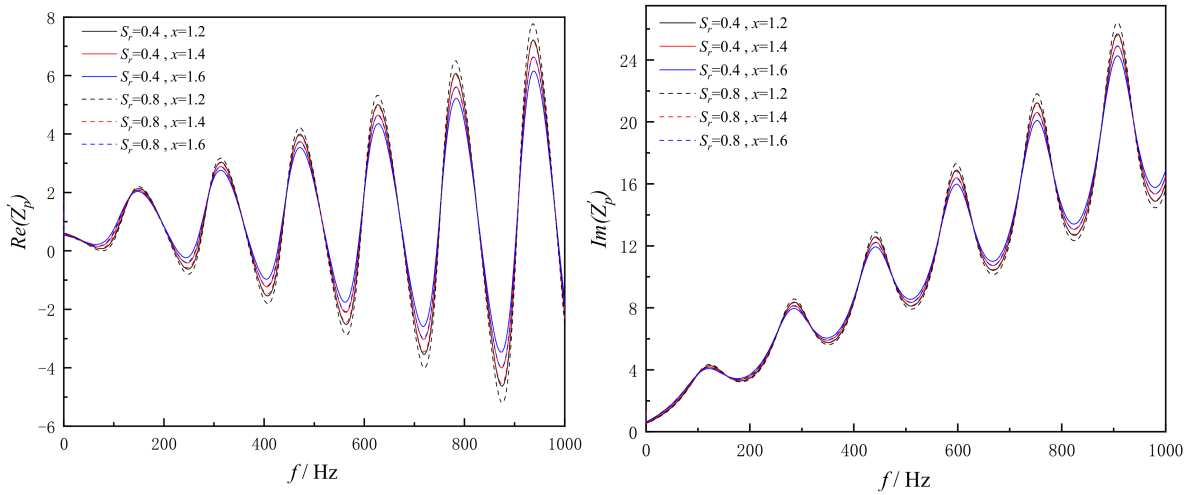


Figure 10. Effects of soil saturation and hardening degree on pile complex impedance.

(3) Effect of construction disturbance for different pile radii

Figures 11 and 12 illustrate how the radial extent of the disturbed soil influences pile-head complex impedance for piles of various radii. As shown in Figure 11, for a given thickness of the softened zone, increasing the pile radius produces higher stiffness and damping response amplitudes. Expansion of the softened region further amplifies both impedance components, and this effect is more pronounced for larger piles. These observations indicate that the influence of softening-zone extent on the pile response becomes stronger as the pile radius increases. An opposite tendency is evident in Figure 12: extending the hardened region reduces the magnitudes of both stiffness and damping, with the attenuation becoming increasingly marked for piles of greater radius.

The combined effects of pile radius and disturbance intensity are presented in Figures 13 and 14. Figure 13 shows that stronger soil softening progressively increases the amplitudes of both impedance components. This amplification grows with pile radius, reflecting an enhanced coupling between pile dimensions and the severity of soil softening. By contrast, Figure 14 demonstrates that greater hardening intensity suppresses the stiffness and damping responses, and the reduction is more substantial for larger piles. Overall, these findings confirm that pile radius significantly modifies the extent to which construction-induced soil disturbance affects the vertical dynamic characteristics of the pile–soil system. Changing the pile radius simultaneously changes the pile cross-sectional

area, the shaft circumference, and the characteristic dimension relative to the soil wavelength. The radius-dependent trends therefore reflect the combined effects of axial pile stiffness, shaft interaction, and wave propagation, rather than the pile–soil material stiffness ratio alone.

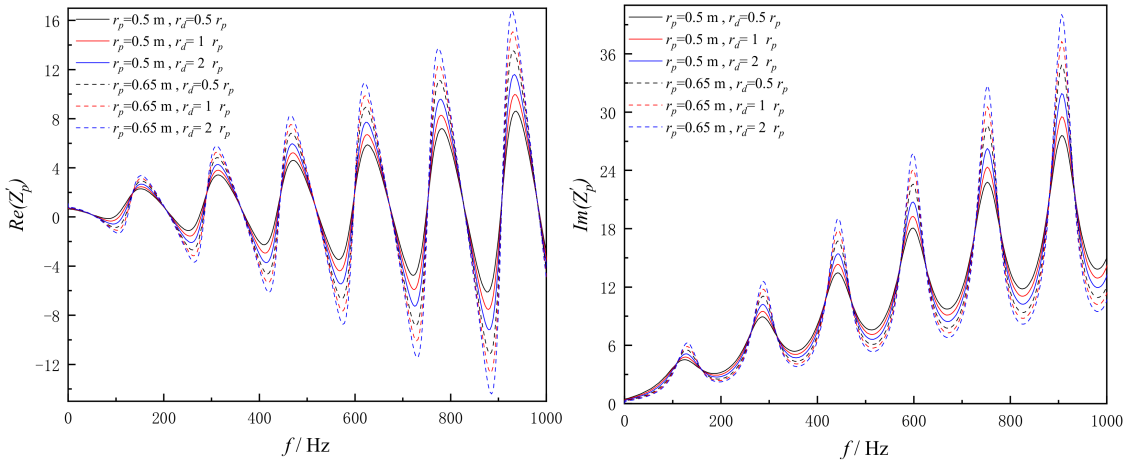


Figure 11. Effects of pile radii and softening range on pile complex impedance.

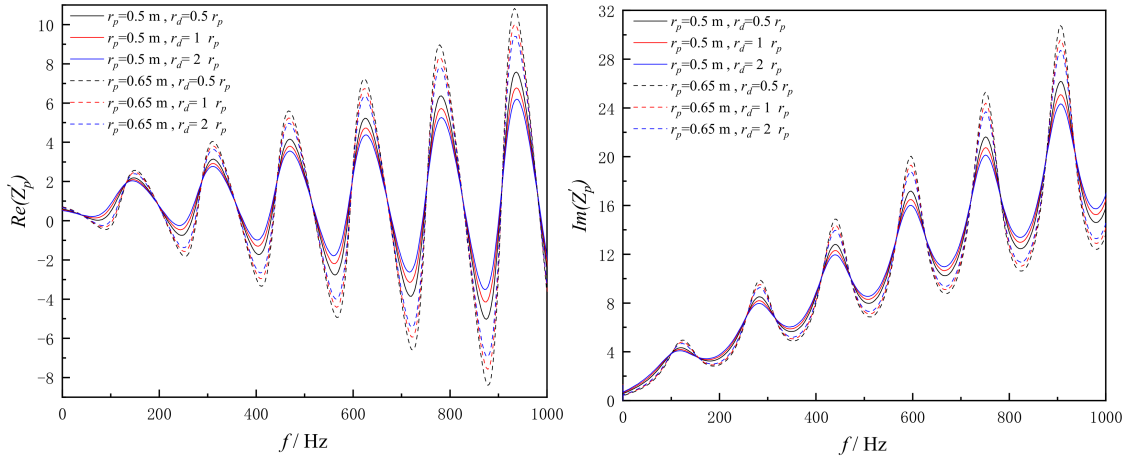


Figure 12. Effects of pile radii and hardening range on pile complex impedance.

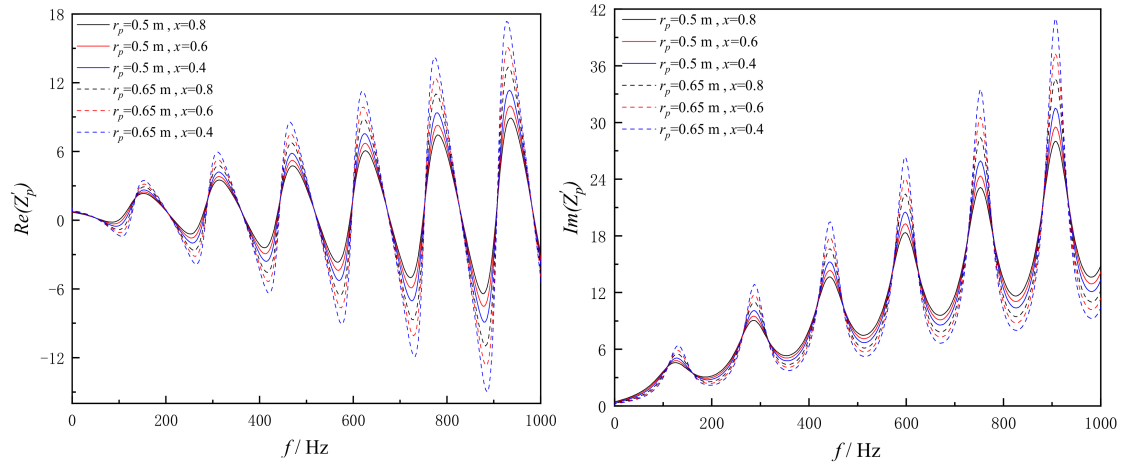


Figure 13. Effects of pile radii and softening degree on pile complex impedance.

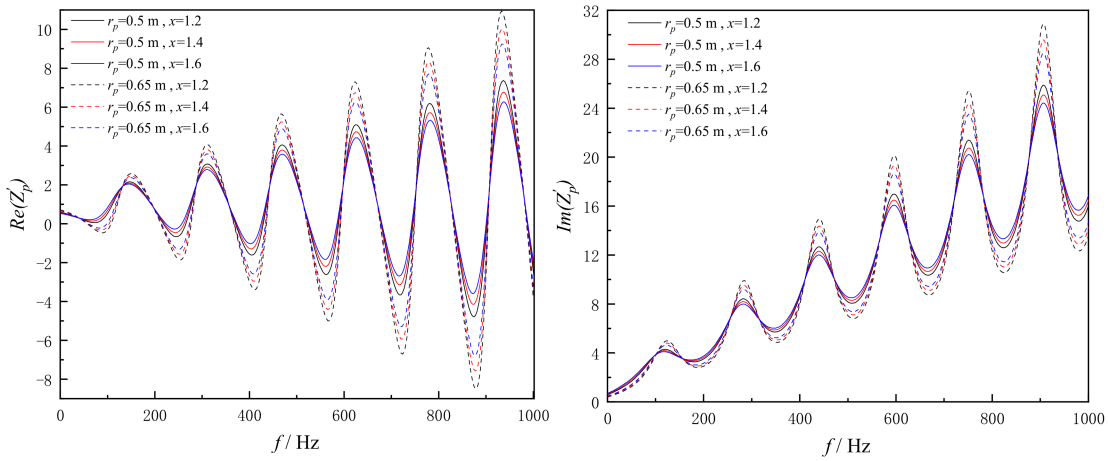


Figure 14. Effects of pile radii and hardening degree on pile complex impedance.

(4) Effect of construction disturbance for different pile elastic moduli

Figures 15 and 16 illustrate the influence of disturbed-zone size on pile-head complex impedance for piles with different elastic moduli. As shown in Figure 15, when the thickness of the softened region is fixed, increasing the pile modulus raises the amplitudes of both dynamic stiffness and damping and shifts the resonance response toward higher frequencies. However, the additional amplification caused by expansion of the softened zone becomes less pronounced as pile stiffness increases. In the hardened-soil case shown in Figure 16, enlarging the disturbed region reduces both impedance components, although this reduction is progressively weakened for stiffer piles.

Figures 17 and 18 further examine the combined effects of disturbance intensity and pile elastic modulus. Figure 17 indicates that stronger soil softening increases the stiffness and damping amplitudes, but the extent of this increase diminishes with increasing pile modulus. Conversely, Figure 18 shows that intensified soil hardening suppresses both impedance components, while the corresponding sensitivity decreases for piles with greater stiffness. Overall, a higher pile elastic modulus tends to lessen the effect of construction-induced soil disturbance on the dynamic impedance response. Increasing the pile elastic modulus raises both the axial rigidity and the longitudinal wave velocity of the pile, providing a physical explanation for the shift of the impedance peaks toward higher frequencies. The reduced sensitivity to soil disturbance indicates that changes in the surrounding soil exert a smaller relative influence when the pile is stiffer.

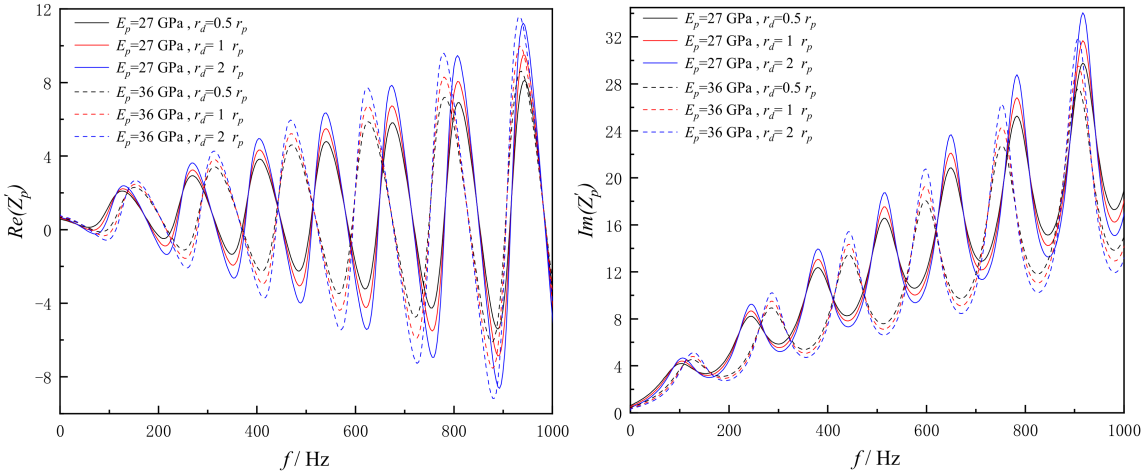


Figure 15. Effects of pile elastic moduli and softening range on pile complex impedance.

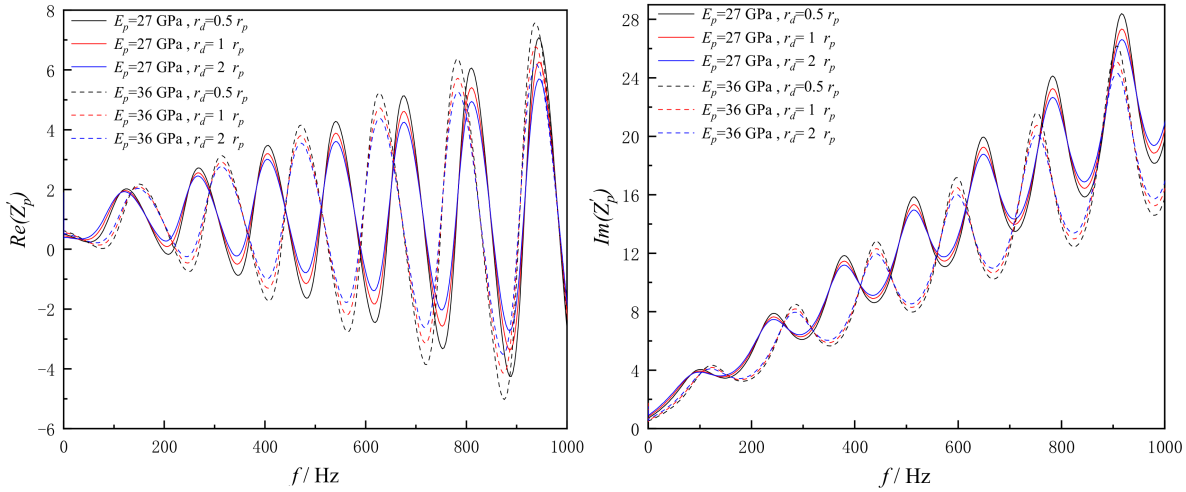


Figure 16. Effects of pile elastic moduli and hardening range on pile complex impedance.

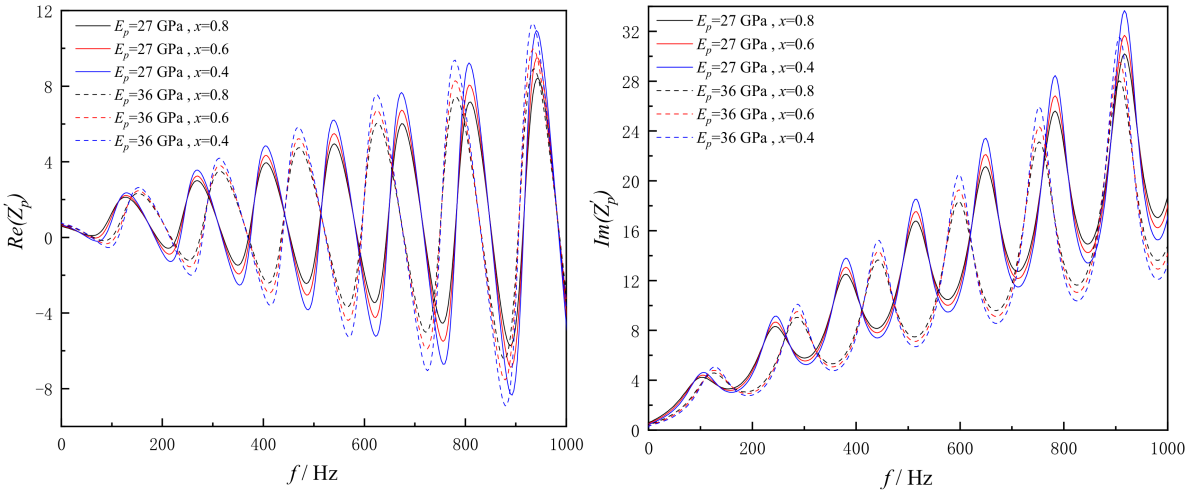


Figure 17. Effects of pile elastic moduli and softening degree on pile complex impedance.

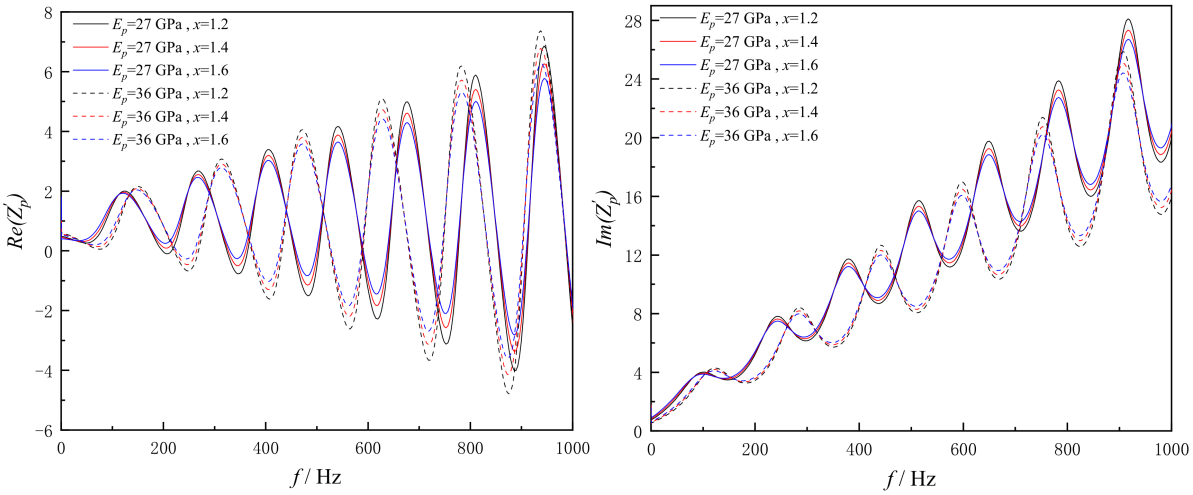


Figure 18. Effects of pile elastic moduli and hardening degree on pile complex impedance.

4.3. Limitations

The model assumes small-amplitude vibration, fully bonded interfaces, and a rigidly restrained pile toe. Construction disturbance is represented only by radial shear-modulus variation; installation-induced hydraulic changes, soil nonlinearity, and skeleton hysteresis are not included. The available convergence checks and analytical comparisons support solution consistency.

5. Conclusions

This study presents an analytical framework for investigating the vertical vibration response of end-bearing piles embedded in unsaturated soils by considering the effects of construction-induced disturbance. The proposed solution is verified in terms of its accuracy and applicability through comparisons with previously published results. The major findings obtained from the parametric analyses are summarized as follows:

(1) Increasing soil saturation from $S_r = 0.4$ to 0.8 enhances the resonance amplitudes of pile-head dynamic stiffness and damping, particularly in the high-frequency range, while producing only minor changes in the corresponding resonance frequencies.

(2) Increasing the disturbed-zone thickness from $0.5r_p$ to $2r_p$, or decreasing the softening coefficient x from 0.8 to 0.4, amplifies the oscillatory stiffness and damping responses at the pile head. Conversely, expansion of the hardened zone or increasing x from 1.2 to 1.6 suppresses these responses. These disturbance-induced variations become more evident at higher excitation frequencies.

(3) Increasing the pile radius from 0.5 to 0.65 m generally increases the pile-head stiffness and damping response amplitudes. Increasing the pile elastic modulus from 27 to 36 GPa also shifts the impedance peaks toward higher frequencies, consistent with the increase in longitudinal wave velocity.

(4) Within the investigated parameter ranges, disturbance-induced impedance variations become more pronounced as soil saturation increases from 0.4 to 0.8 and pile radius increases from 0.5 to 0.65 m. In contrast, increasing the pile elastic modulus from 27 to 36 GPa reduces the influence of disturbance, reflecting the increased axial rigidity of the pile.

Author Contributions: C.Z.: methodology, formal analysis, resources, supervision, funding acquisition, project administration, conceptualization. R.L.: software, validation, formal analysis, writing—review and editing, writing—original draft, data curation, funding acquisition. P.W.: supervision, funding acquisition, project administration, resources, conceptualization. L.W.: conceptualization, resources, project administration, supervision. Z.L.: conceptualization, methodology, validation, supervision, visualization, resources, software, formal analysis, writing—review and editing. All authors have read and agreed to the published version of the manuscript.

Funding: This research was supported by the Graduate Education Innovation Program of Xizang Agriculture and Animal Husbandry University (SGYC2026002), the Science and Technology Projects of Xizang Autonomous Region, China (Grant Nos. XZ202401JD0005; XZ202601ZY0088).

Institutional Review Board Statement: Not applicable.

Informed Consent Statement: Not applicable.

Data Availability Statement: The data presented in this study are available upon request from the corresponding author. The data are not publicly available due to privacy.

Conflicts of Interest: The authors declare no conflicts of interest.

Abbreviations

Symbol	Definition	Unit
H	Pile length	m
r_p	Pile radius	m
r	Radial coordinate	m
z	Vertical coordinate	m
r_j	Inner radius of the jth annular soil region	m
m	Number of annular regions in the radial discretization	—
j	Annular-region index	—
x	Disturbance coefficient defined in Section 4	—
S_r	Degree of saturation	—
n	Soil porosity	—
G_s	Shear modulus of the soil skeleton	Pa
μ	Reference saturated-soil shear modulus in the adopted modulus–saturation relationship	Pa
K_s	Bulk modulus of soil particles	Pa
K_f	Bulk modulus of pore water	Pa
K_g	Bulk modulus of pore gas	Pa
K_b	Bulk modulus of the soil skeleton	Pa
K_d	Intrinsic permeability	m^2
k_{rf}	Relative permeability coefficient of pore water	—
k_{rg}	Relative permeability coefficient of pore gas	—
u	Soil-skeleton displacement vector	m
v	Pore–water displacement vector relative to the skeleton	m
w	Pore–gas displacement vector relative to the skeleton	m
P_0	Amplitude of the harmonic force applied at the pile head	N
f	Excitation frequency	Hz
ω	Angular frequency	rad s^{-1}
t	Time	s

References

1. Wang, J.; Zhou, D.; Zhang, Y.Q.; Cai, W. Vertical Impedance of a Tapered Pile in Inhomogeneous Saturated Soil Described by Fractional Viscoelastic Model. *Appl. Math. Model.* **2019**, *75*, 88–100. [CrossRef]
2. Sawamura, Y.; Inagami, K.; Nishihara, T.; Kosaka, T.; Hattori, M.; Kimura, M. Seismic Performance of Group Pile Foundation with Ground Improvement during Liquefaction. *Soils Found.* **2021**, *61*, 944–959. [CrossRef]
3. Liu, Q.J.; Zhang, Y.Q.; Gao, W.H. A Mechanistic Insight into the Shaft Resistance of Vertically Vibrating Piles. *Soils Found.* **2019**, *59*, 97–109. [CrossRef]
4. Qu, L.M.; Ding, X.M.; Kouroussis, G.; Zheng, C.J. Dynamic Interaction of Soil and End-Bearing Piles in Sloping Ground: Numerical Simulation and Analytical Solution. *Comput. Geotech.* **2021**, *134*, 103917. [CrossRef]
5. Meng, K.; Su, H.F. Analytical Model of Large-Diameter Viscoelastic Floating Pile and Application in Pile Low-Strain Integrity Testing. *Soil Dyn. Earthq. Eng.* **2022**, *158*, 107296. [CrossRef]
6. Liu, H.; Wu, W.B.; Yang, X.Y.; Liu, X.; Wang, L.X.; Naggar, M.H.E.; Wen, M.J. Apparent Wave Velocity Inverse Analysis Method and Its Application in Dynamic Pile Testing. *Int. J. Numer. Anal. Methods Geomech.* **2023**, *47*, 549–569. [CrossRef]
7. Wu, J.T.; Wang, K.H.; El Naggar, M.H. Dynamic Soil Reactions around Pile-Fictitious Soil Pile Coupled Model and Its Application in Parallel Seismic Method. *Comput. Geotech.* **2019**, *110*, 44–56. [CrossRef]
8. Luan, L.B.; Zheng, C.J.; Kouretzis, G.; Ding, X.M.; Poulos, H. A New Dynamic Interaction Factor for the Analysis of Pile Groups Subjected to Vertical Dynamic Loads. *Acta Geotech.* **2020**, *15*, 3545–3558. [CrossRef]
9. Shi, L.; Xu, C.J.; Cai, Y.Q.; Geng, X.Y. Dynamic Impedances and Free-Field Vibration Analysis of Pile Groups in Saturated Ground. *J. Sound Vib.* **2014**, *333*, 3709–3731. [CrossRef]
10. Ai, Z.Y.; Wang, L.H. Effect of Compressible Parameters on Vertical Vibration of an Elastic Pile in Multilayered Poroelastic Media. *Comput. Geotech.* **2017**, *89*, 195–202. [CrossRef]
11. Li, Y.; Ai, Z.Y. Horizontal Transient Response of a Pile Group Partially Embedded in Multilayered Transversely Isotropic Soils. *Acta Geotech.* **2021**, *16*, 335–346. [CrossRef]
12. Anoyatis, G.; Mylonakis, G. Dynamic Winkler Modulus for Axially Loaded Piles. *Géotechnique* **2012**, *62*, 521–536. [CrossRef]
13. Ding, X.M.; Liu, H.L.; Kong, G.Q.; Zheng, C.J. Time-Domain Analysis of Velocity Waves in a Pipe Pile Due to a Transient Point Load. *Comput. Geotech.* **2014**, *58*, 101–116. [CrossRef]

14. Liu, H.; Wu, W.B.; Jiang, G.S.; El Naggar, M.H.; Mei, G.X.; Liang, R.Z. Influence of Soil Plug Effect on the Vertical Dynamic Response of Large Diameter Pipe Piles. *Ocean Eng.* **2018**, *157*, 13–25. [CrossRef]
15. Novak, M.; Sachs, K. Torsional and Coupled Vibrations of Embedded Footings. *Earthq. Engng Struct. Dyn.* **1973**, *2*, 11–33. [CrossRef]
16. Zheng, C.J.; Kouretzis, G.P.; Ding, X.M.; Liu, H.L.; Poulos, H.G. Three-Dimensional Effects in Low-Strain Integrity Testing of Piles: Analytical Solution. *Can. Geotech. J.* **2016**, *53*, 225–235. [CrossRef]
17. Luan, L.B.; Ding, X.M.; Zheng, C.J.; Kouretzis, G.; Wu, Q. Dynamic Response of Pile Groups Subjected to Horizontal Loads. *Can. Geotech. J.* **2020**, *57*, 469–481. [CrossRef]
18. Nogami, T.; Novak, M. Soil-pile Interaction in Vertical Vibration. *Earthq. Engng Struct. Dyn.* **1976**, *4*, 277–293. [CrossRef]
19. Cui, C.Y.; Meng, K.; Xu, C.S.; Liang, Z.M.; Li, H.J.; Pei, H.F. Analytical Solution for Longitudinal Vibration of a Floating Pile in Saturated Porous Media Based on a Fictitious Saturated Soil Pile Model. *Comput. Geotech.* **2021**, *131*, 103942. [CrossRef]
20. Li, Z.Y.; Zhao, C.H.; Xi, Y.Q.; Jin, N.N.; Gao, Y.F. Torsional Vibration of a Pile in Unsaturated Soil Considering the Construction Disturbance. *Comput. Geotech.* **2024**, *172*, 106409. [CrossRef]
21. Wang, K.H.; Wu, W.B.; Zhang, Z.Q.; Leo, C.J. Vertical Dynamic Response of an Inhomogeneous Viscoelastic Pile. *Comput. Geotech.* **2010**, *37*, 536–544. [CrossRef]
22. Cui, C.Y.; Meng, K.; Wu, Y.J.; Chapman, D.; Liang, Z.M. Dynamic Response of Pipe Pile Embedded in Layered Visco-Elastic Media with Radial Inhomogeneity under Vertical Excitation. *Geomech. Eng.* **2018**, *16*, 609–618. [CrossRef]
23. Zhang, N.; Wang, L.; Zhang, Y.; Lu, H.J.; Dai, D.H.; Cai, G.J.; Gao, Y.F. Effect of a V-shaped Canyon on the Seismic Response of a Bridge under Oblique Incident SH Waves. *Earthq. Engng Struct. Dyn.* **2024**, *53*, 496–514. [CrossRef]
24. Zheng, C.J.; Hua, J.M.; Ding, X.M. Torsional Vibration of a Pipe Pile in Transversely Isotropic Saturated Soil. *Earthq. Eng. Eng. Vib.* **2016**, *15*, 509–517. [CrossRef]
25. Wang, B.L.; Cui, C.Y.; Xu, C.S.; Meng, K.; Li, J.B.; Xu, L.N. A Novel Analytical Solution for Horizontal Vibration of Partially Embedded Offshore Piles Considering the Distribution Effect of Wave Loads. *Ocean Eng.* **2024**, *307*, 118179. [CrossRef]
26. Wang, B.L.; Liu, H.L.; Cui, C.Y.; Liang, Z.M.; Li, J.B.; Xu, C.S. A New Closed-Form Solution for Horizontal Vibration of Offshore Piles in Layered Saturated Seabed Subjected to Wave Loads. *Ocean Eng.* **2026**, *343*, 123347. [CrossRef]
27. Mikhailov, D.N. The Influence of Gas Saturation and Pore Pressure on the Characteristics of the Frenkel-Biot P Waves in Partially Saturated Porous Media. *Izv. Phys. Solid Earth* **2010**, *46*, 897–909. [CrossRef]
28. Lu, N.; Likos, W.J. Suction Stress Characteristic Curve for Unsaturated Soil. *J. Geotech. Geoenviron. Eng.* **2006**, *132*, 131–142. [CrossRef]
29. Biot, M.A. Theory of Propagation of Elastic Waves in a Fluid-Saturated Porous Solid. I. Low-Frequency Range. *J. Acoust. Soc. Am.* **1956**, *28*, 168–178. [CrossRef]
30. Wang, X.H.; Zhang, M. Dynamical Response of Vertically Loaded Pile in Half-Space of Unsaturated Porous Media. *Chin. J. Geotech. Eng.* **2013**, *35*, 1210–1220.
31. Guo, P.F.; Zhou, S.H.; Yang, L.C.; Xiao, J.H. Analytical Solution of the Vertical Dynamic Response of Rock-Socketed Pile Considering Transverse Inertial Effect in Unsaturated Soil. *Chin. J. Theor. Appl. Mech.* **2017**, *49*, 113–127.
32. Shan, Y.; Ma, W.J.; Xiang, K.; Wang, B.L.; Zhou, S.H.; Guo, H.J. Vertical Dynamic Response of a Floating Pile in Unsaturated Poroelastic Media Based on the Fictitious Unsaturated Soil Pile Model. *Appl. Math. Model.* **2022**, *109*, 209–228. [CrossRef]
33. Ma, W.J.; Shan, Y.; Xiang, K.; Wang, B.L.; Zhou, S.H. Vertical Dynamic Impedance of End-bearing Pile Groups Embedded in Homogeneous Unsaturated Soils. *Int. J. Numer. Anal. Methods Geomech.* **2022**, *46*, 1154–1176. [CrossRef]
34. Fu, P.; Xie, K.H. Lateral Vibration of Offshore Piles Considering Pile-Water Interaction. *Int. J. Str. Stab. Dyn.* **2019**, *19*, 1950147. [CrossRef]
35. Wu, W.B.; Yang, Z.J.; Liu, X.; Zhang, Y.P.; Liu, H.; El Naggar, M.H.; Xu, M.J.; Mei, G.X. Horizontal Dynamic Response of Pile in Unsaturated Soil Considering Its Construction Disturbance Effect. *Ocean Eng.* **2022**, *245*, 110483. [CrossRef]
36. Zou, X.J.; Yang, Z.J.; Wu, W.B. Horizontal Dynamic Response of Partially Embedded Single Pile in Unsaturated Soil under Combined Loads. *Soil. Dyn. Earthq. Eng.* **2023**, *165*, 107672. [CrossRef]
37. Li, J.B.; Cui, C.Y.; Xiao, Z.S.; Wang, B.L.; Xu, C.S. Reliability and Sensitivity Analyses of Monopile Supported Offshore Wind Turbines Based on Probability Density Evolution Method with Pre-Screening of Controlling Parameters. *Ocean Eng.* **2024**, *310*, 118746. [CrossRef]
38. Li, J.B.; Liu, H.L.; Cui, C.Y.; Yuan, L.S.; Ji, Z.Z.; Xu, C.S. Reliability Analysis of Monopile-Supported Offshore Wind Turbines Considering Load Correlations and Multi-Source Uncertainties under Data Scarcity Conditions. *Ocean Eng.* **2026**, *353*, 124851. [CrossRef]
39. Ma, W.J.; Shan, Y.; Xiang, K.; Wang, B.L.; Zhou, S.H. Torsional Dynamic Response of a Pipe Pile in Homogeneous Unsaturated Soils. *Comput. Geotech.* **2022**, *143*, 104607. [CrossRef]
40. Ma, W.J.; Shan, Y.; Wang, B.L.; Zhou, S.H.; Wang, C.D. Analytical Solution for Torsional Vibration of an End-Bearing Pile in Nonhomogeneous Unsaturated Soil. *J. Build. Eng.* **2022**, *57*, 104863. [CrossRef]

41. Li, Z.Y.; Zhao, C.H.; Gao, Y.F.; Wu, W.B.; Wang, K.H.; Zhang, Z.Q. Torsional Vibration of a Floating Pile in Radially Inhomogeneous Unsaturated Soil Based on the Fictitious Unsaturated Soil Pile Model. *Soil. Dyn. Earthq. Eng.* **2024**, *183*, 108812. [CrossRef]
42. Zhao, C.H.; Li, Z.Y.; Zhang, C.; Zhang, Z.Q. Torsional Vibration of Rock-Socketed Piles Considering the Bottom Sediment and Construction Disturbance. *Int. J. Str. Stab. Dyn.* **2026**, *26*, 2650037. [CrossRef]
43. Zhang, N.; Zhang, Y.; Gao, Y.F.; Pak, R.Y.S.; Yang, J. Site Amplification Effects of a Radially Multi-Layered Semi-Cylindrical Canyon on Seismic Response of an Earth and Rockfill Dam. *Soil Dyn. Earthq. Eng.* **2019**, *116*, 145–163. [CrossRef]
44. Han, Y.C.; Sabin, G.C.W. Impedances for Radially Inhomogeneous Viscoelastic Soil Media. *J. Eng. Mech.* **1995**, *121*, 939–947. [CrossRef]
45. El Naggar, M.H. Vertical and Torsional Soil Reactions for Radially Inhomogeneous Soil Layer. *Struct. Eng. Mech.* **2000**, *10*, 299–312. [CrossRef]
46. Wang, P.G.; Xu, Y.D.; Zhang, X.L.; Xi, R.Q.; Du, X.L. A Substructure Method for Seismic Responses of Offshore Wind Turbine Considering Nonlinear Pile-Soil Dynamic Interaction. *Soil Dyn. Earthq. Eng.* **2021**, *144*, 106684. [CrossRef]
47. Li, Z.Y.; Chen, Y.; Gao, Y.F.; Zhang, Z.Q. Longitudinal Vibration of Large-Diameter Piles in Transversely Isotropic Soil Considering Three-Dimensional Pile Effects. *Soil Dyn. Earthq. Eng.* **2026**, *209*, 110406. [CrossRef]
48. Yang, D.Y.; Wang, K.H.; Zhang, Z.Q.; Leo, C.J. Vertical Dynamic Response of Pile in a Radially Heterogeneous Soil Layer. *Int. J. Numer. Anal. Methods Geomech.* **2009**, *33*, 1039–1054. [CrossRef]
49. Cai, Y.Y.; Liu, Z.H.; Li, T.B.; Yu, J.; Wang, N. Vertical Dynamic Response of a Pile Embedded in Radially Inhomogeneous Soil Based on Fictitious Soil Pile Model. *Soil Dyn. Earthq. Eng.* **2020**, *132*, 106038. [CrossRef]
50. Li, Z.Y.; Jin, N.N.; Xian, R.; Gao, Y.F.; Zhang, C.; Wu, W.B.; Zhang, Z.Q. Torsional Vibration of a Tapered Pipe Pile Considering the Circumferential Support Exerted by the External and Internal Soils. *Soil Dyn. Earthq. Eng.* **2025**, *198*, 109558. [CrossRef]
51. Li, Z.Y.; Zhao, C.H.; Wang, Z.J.; Zhang, C.; Zhang, Z.Q. Torsional Vibration of a Pipe Pile in Layered Unsaturated Soil Considering the Construction Disturbance. *Ocean Eng.* **2025**, *340*, 122287. [CrossRef]
52. Fu, P. Horizontal Dynamic Response of an Offshore Pile in Saturated Soil Considering Radial Inhomogeneity. *Int. J. Str. Stab. Dyn.* **2025**, *25*, 2550249. [CrossRef]
53. Li, Z.Y.; Gao, Y.F.; Wang, K.H. Vertical Vibration of an End Bearing Pile Interacting with the Radially Inhomogeneous Saturated Soil. *Ocean Eng.* **2021**, *219*, 108009. [CrossRef]
54. Xu, M.J.; Wei, D.M. 3D Non-Axisymmetrical Dynamic Response of Unsaturated Soils. *Eng. Mech.* **2011**, *28*, 78–85.

Disclaimer/Publisher's Note: The statements, opinions and data contained in all publications are solely those of the individual author(s) and contributor(s) and not of MDPI and/or the editor(s). MDPI and/or the editor(s) disclaim responsibility for any injury to people or property resulting from any ideas, methods, instructions or products referred to in the content.